Chapter 5
The relationship between interannual climatic change and interannual change in net carbon budget of terrestrial ecosystems

5.1. Introduction

The terrestrial ecosystems play a critical role in the global carbon cycle (Bolin et al., 1979). However, in spite of a large amount of effort, we can hardly quantify the extent of the terrestrial ecosystem net carbon sink, and how it will change in the future. We should take three major effects into account at the global scale: the ongoing CO_2 enrichment, climate change, and human land-use change. The anthropogenic CO_2 emission has steadily increased the atmospheric CO_2 concentration since the pre industrial revolution age, and then it exerts a monotonous, although non linear, fertilization effect on the ecosystem carbon cycle (Melillo et al., 1996). The human land-use change may be the most complicated factor to predict, but qualitatively this effect has reduced and will continue to reduce carbon storage of the biosphere (Houghton et al., 1998). However, the impacts of climate change on the biosphere, even their direction, are less clear for the following reasons. (1) Climate influences various ecosystem processes simultaneously. (2) A number of climatic factors, such as temperature, precipitation, and irradiance, change concurrently and affect ecosystem processes interactively. (3) Spatial variability of the climatic anomaly is large and scale-dependent. (4) Several fluctuations that have different time scales are multiplicatively combined in the observed climate records.

In this study, we put emphasis on the effect of interannual (i.e. year-to-year) climatic perturbations, so that we may address the environmental dependency of the atmosphere-biosphere CO_2 exchange. An El Niño and Southern Oscillation (ENSO) event represents the most obvious interannual climate change, and often accompanies regionally warmer temperatures and lower precipitation (Ropelewski and Halpert, 1987; Halpert and Ropelewski,

1992). Also, a huge volcanic eruption can lead to attenuated direct solar radiation and cooler surface temperatures (Robock and Mao, 1995). These evident perturbations may have an influence on ecosystem productivity at the broad scale, as observed by remote sensing (Myneni et al., 1997).

The short-term impact of climate change on ecosystems should be mainly regulated by a couple of physiological processes, and then we can describe the impacts with an ecophysiology-based model. Although the atmosphere-biosphere CO_2 exchange is partly affected by such disturbance processes as fire and deforestation, we focus only on those processes regulated at the physiological level, such as photosynthesis, respiration, and decomposition. Other processes, in particular biomass burning, may have a substantial contribution not only at the local scale but also at the continental scale, and they have been addressed by other studies (e.g. Wittenberg et al., 1998).

In this chapter, Sim-CYCLE simulates the time-series of atmosphere-biosphere CO_2 exchange during the period from 1958 to 1998, and analyzes the relationship between the climate perturbations and the anomalies in the terrestrial carbon budget, especially in net ecosystem production (ΔNEP), which indicates whether an ecosystem acted as a net carbon sink or a source during a given period. Then, it is discussed whether the estimated ΔNEP could have an influence to such an extent that it contributed to the observed anomalies in the atmospheric CO_2 concentration (Nakazawa et al., 1991; Keeling et al., 1995) (Fig. 5-1). Indeed, this issue has attracted the attention of researchers of global carbon cycle models (e.g. Dai and Fung, 1993; Kaduk and Heimann, 1994; Maisongrande et al., 1995; Kindermann et al., 1996; Gérard et al., 1999; Potter et al., 1999; Rayner and Law, 1999).

5. 2. Climate dataset

The climate condition for the model analysis is derived from the reanalysis dataset produced by the U.S. National Centers for Environmental Prediction and the National Center for Atmospheric Research (NCEP/NCAR). This is a gridded dataset in which observation records were interpolated by the four dimensional data assimilation method (Kalnay et al.,

1996). In this stage, the monthly composite dataset is supplied for 41 years, from Jan. 1958 to Dec. 1998; we took this interval to be the experimental period. In the NCEP/NCAR-reanalysis dataset, surface variables are arranged on a Gaussian grid of T62 resolution (94 x 192 latitude-longitude grid cells), which seems likely to be sufficiently fine for the purpose of global analysis; we took this resolution to be the spatial resolution of simulation in this research. The carbon budget was calculated autonomously for each of 5,828 terrestrial grid points.

The advantage of adopting the reanalysis dataset is, we postulate, due to the climatological consistency and homogeneous accuracy throughout the experimental period. In addition, the NCEP/NCAR reanalysis dataset provides a larger number of diagnostic variables than those derived from simple interpolation of observations (e.g. Leemans and Cramer, 1991; New et al., 1999). The following variables were adopted for our model analysis: surface downward shortwave radiation fluxes (*RTG*, in W m^{-2}): ground surface air temperature (*TG*, in °C): soil temperatures at 10 and 200 cm in depths (TS_{10} and TS_{200}, in °C): potential evapotranspiration rate (*PET*, in W m^{-2}): latent heat flux (i.e. actual evapotranspiration rate, *AET* in W m^{-2}): and volumetric soil moisture contents at 10 and 200 cm in depths (MS_{10} and MS_{200}, in fraction). Additionally, the monthly precipitation (*PR*, in mm mon^{-1}), although not a model input, is used later in the regression analysis between the simulation outcome and climatic factors. In the simulation analysis, the irradiance of PAR at the canopy-top $PPFD_{SFC}$ (μmol photon m^{-2} s^{-1}) was derived from the NCEP/NCAR-reanalysis data:

$$PPFD_{SFC} = 4.2 \cdot (RTG \cdot 0.45) \qquad (5\text{-}1)$$

where multipliers 4.2 and 0.45 are for unit conversion from W m^{-2} to μmol photon m^{-2} s^{-1}, and for extraction of the fraction of PAR, respectively (Larcher, 1995).

A climatic anomaly is defined as the difference from the 41-year average value, and was used for linear and multiple regression analyses with the carbon flux anomalies. Before the multiple regression analysis, mutual correlations among the climatic components were checked to specify a combination of independent variables.

5.3. Simulation design

The biome distribution for the global simulation was derived from the mapping by Matthews et al. (1983), for both potential biome and cultivation intensity. In our model analysis (Fig. 5-2), the spatial resolution of the original dataset, i.e. 1-degree latitude-longitude, was adjusted to that of the NCEP/NCAR-reanalysis by resampling the grid points, and the natural biome category, i.e. 32 types of the original, was simplified into 12 types (Table 5-1). From the cultivation intensity in the dataset, we can estimate the general extent of the human land-use change, although we did not include the additional deforestation during the experimental period. In croplands, a constant fraction on plant biomass is harvested; the difference between *NEP* and harvested carbon is termed net carbon balance (*NCB*). In arid rangelands including savanna, grassland, and desert (biomes 7, 8, and 11 in Table 5-1), calculation of C_3 and C_4 plants is separately carried out because of their significant differences in photosynthetic capacity and sensitivities to temperature, aridity, and CO_2 conditions. The ecophysiological discrepancies between C_3 and C_4 species are reflected in their geographical distribution (C_4 species have larger predominance in lower and warmer latitudes), and may have a notable importance under global change conditions (Collatz et al., 1998). The C_3/C_4 composition in arid rangeland grids was empirically estimated by a regression model relating the composition with latitude (e.g. review by Sage et al., 1999; Teeri and Stowe, 1976; Ehleringer et al., 1997). Several representative parameters and average climate condition are shown in Table 5-2 and Table 5-3, respectively.

For each grid point, simulation began from a juvenile stage of ecosystem with a little carbon storage (0.1 Mg C ha^{-1} for each compartment), and through the iterative calculation (4100 years) the carbon budget was to be fully stabilized so as to reach the climax stage, where annual *NEP* is equal to zero. On the other hand, in cultivated areas, a typical cultivation cycle from spring planting to autumn harvesting was modeled. The calculations were performed under a stationary atmospheric CO_2 level: 316.1 ppmv, that is, the background level in 1958 (WDCGG, 1998). Consequently, we obtain the equilibrium carbon budget both

in natural and in agricultural ecosystems at the beginning of the simulation; this made it tractable to analyze the interannual change in the terrestrial carbon budget.

After that, the real simulation from 1958 to 1998 was carried out using the actual climatic and atmospheric CO_2 conditions. During the experimental period, the atmospheric CO_2 concentration increased at the rate of approximately +1.4 ppmv per year, from 316.1 to 367.3 ppmv (WDCGG, 1998). Note that we focused on the effect of climate perturbations, although the actual and modeled ecosystem carbon dynamics are sensitive to the atmospheric CO_2 level. Exploring the effects of CO_2 fertilization on the global carbon cycle remains to be done by our next research. Then, to remove the trend induced by the CO_2 fertilization effect from the bulk trend (cf. Fig. 5-14a), a supplementary simulation using the actual CO_2 increase and the average stationary climate condition was performed (cf. Fig. 5-14b).

$$\Delta F_{bulk} = F_{bulk} - \overline{F_{bulk}} \tag{5-2a}$$

$$\Delta F_{CO2} = F_{CO2} - \overline{F_{CO2}} \tag{5-2b}$$

where F represents *GPP*, *AR*, *NPP*, *HR*, or *NEP*. Fbulk and F_{CO2} denote the carbon fluxes calculated by simulations using the actual and average climate data, respectively (a line over symbol indicates the 41-year arithmetic mean). By comparing these two trends, we clarified the climate-induced short-term anomalies in terrestrial carbon flux ΔF (cf. Fig. 5-14c), which takes the form:

$$\Delta F = \Delta F_{bulk} - \Delta F_{CO2} \tag{5-2c}$$

Most of analyses in this paper deal with this carbon flux anomaly.

Modeling of the environmental dependencies is a critical point for the simulation research of carbon exchange processes. Then, Sim-CYCLE incorporates the environmental dependencies on the basis of physiological responses, i.e. at the scale of organs such as a single leaf, where a large amount of observations and experiments have been accumulated.

Below, we present brief descriptions of carbon fluxes and their dependencies on light, temperature, and water conditions. The physiological regulation is firstly described, and scaling-up to the ecosystem-level regulation of the carbon budget was done next.

5. 4. Environmental sensitivity of CO_2 exchange

5. 4. 1. Light conditions

Photosynthesis is the sole carbon exchange process dependent directly on light condition (Fig. 5-4a). A large number of studies which addressed the relationship between irradiance and canopy-level production show that generally *GPP* needs a much stronger irradiance for light-saturation than single-leaf photosynthesis (cf. review by Ruimy et al., 1995). This suggests that canopy *GPP* is still sensitive to $PPFD_{SFC}$ during growing-periods (Fig. 5-4a). Except for orbital factors making seasonal and diurnal cycles, the surface irradiance may be influenced by cloudiness and atmospheric optical thickness, related to air dust and aerosol content.

5.4.2. Temperature condition

All of the atmosphere-biosphere CO_2 exchange processes are sensitive to temperature change in different fashions (Fig. 5-4b). In this chapter, the TG-HR relationship was formulated by an exponential function, instead of Eq. 2-63, in order to perform a sensitivity analysis with respect to Q_{10} value. The sensitivity of *NPP* and *NEP* at the ecosystem level can be deduced from those of *GPP*, *AR*, and *HR* (Fig. 5-4b). Fitter and Hay (1981) showed that the temperature-*NPP* relationship is well described by a bell-shape curve, whose optimum temperature is lower than that of the temperature-*GPP* relationship (T_{OPT} of Eq. 2-45). The temperature-*NEP* relationship is also well described by a bell-shape curve with an even lower optimum temperature than the *NPP* one. Actually, a warmer temperature accelerates evapotranspiration and reduces soil water content, and it may consequently affect plant production and soil decomposition (described next). This complexity resulting from the water-temperature interaction gives an additional motivation to adopt a process-based model,

rather than an empirical model.

5.4.3. Water and CO_2 conditions

All of the atmosphere-biosphere CO_2 exchange processes are directly and indirectly sensitive to habitat water condition, and many ecosystems suffer from chronic or periodic water deficit. It was assume that water availability firstly regulates the aperture of leaf stomata, through which plants exchange CO_2 and water simultaneously (Jones, 1992). An empirical indicator, i.e. the ratio of actual evapotranspiration rate to the potential rate (*AET/PET*), is derived directly from the NCEP/NCAR-reanalysis dataset. For example, as shown in Fig. 5-4c, if the *AET/PET* ratio is nearly zero under a dry condition, leaf stomatal conductance (*GS*, in mmol CO_2 m^{-2} s^{-1}) is minimized so that plants do not lose water by transpiration. In contrast, if the *AET/PET* ratio is nearly unity, the soil is sufficiently wet and plants maximize stomatal conductance and CO_2 uptake. Under intermediate moisture conditions, stomatal aperture is estimated by linear interpolation between the maximum (*AET/PET*=1) and minimum (*AET/PET*=0) stomatal conductances (Table 5-2).

As shown by Lieth (1975) on the ecosystem level, the annual precipitation-*NPP* relationship may be well described by a saturation curve from desert to rain forest. At the physiological level, the water-CD_{ICL} and CD_{ICL}-*PC* relationships formulated as hyperbolic functions (Eqs. 2-47 and 2-49) imply that the water-*NPP* relationship is well described by a saturation curve (Fig. 5-4c). However, an enhanced *GPP* leads to a more growth respiration (*ARG*), and offsets a part of the *NPP* increase, while maintenance respiration (*ARM*) is independent of water condition. Here, we should also take account of the temperature-water interaction; that is, a warmer temperature usually results in greater *PET*, but not usually in greater *AET*. Under certain conditions, even if temperature is below the optimum for production, a warmer temperature may aggravate water stress (i.e. smaller *AET/PET* ratio, *GS*, and CD_{ICL}) and decrease *GPP* and *NPP*.

In consequence, both the water-*NPP* and water-*HR* relationships take a hyperbolic-type dependence, and then the water-*NEP* relationship is not intuitive, because it is the net

balance of *NPP* and *HR* offsetting each other. Although precipitation is one of the most changeable factors at the seasonal and interannual scales, causing local droughts and floods, a large water pool in groundwater and plant biomass often ameliorates the perturbation of water availability. On the other hand, an anomalously excess precipitation will persist in soil water content for the next few months (Manabe and Wetherald, 1987). The history effect is a characteristic of the water condition, making it difficult to estimate the impact of its fluctuation on carbon budget.

5.5. Results

At first, state of the climatic condition during the experimental period is described in section 5.5.1. Then, the equilibrium carbon budget is described in section 5.5.2, and interannual change during the 41 years, accounting for the sensitivity to Q_{10} values, is illustrated in section 5.5.3. In sections 5.5.4 and 5.5.5, carbon budget anomalies are statistically related to climatic anomalies through the 41 years. To facilitate discussion, the grid-based estimations are conveniently grouped into five latitudinal zones (Z1 to Z5, cf. Table 5-1) and twelve biome types. Finally, typical features of the carbon anomaly are exemplified with examples in section 5.5.6.

5.5.1. Environmental conditions from 1958 to 1998

Global climate of the NCEP/NCAR-reanalysis exhibited substantial temporal fluctuations. As shown in Fig. 5-5, the time-series of the anomaly of monthly mean land temperature (ΔTG, SD=±0.363 °C) shows the largest positive one in July 1998 (+1.13 °C above the long-term average), and the largest negative one in Feb. 1974 (–1.09 °C below). Apparently, 1998 was the warmest year in the experimental period, such that annual average land temperature was +0.58 °C above the long-term average (9.2±0.23 °C; Table 5-4). The terrestrial warmth was especially evident in North America, Monsoon Asia, eastern Siberia, part of Africa, and the equatorial Pacific region (cf. Fig. 5-26a). Monthly global land precipitation (Fig. 5-6) also showed perturbations (ΔPR, SD=±2.94 mm mon^{-1}), ranging from

+10.4 mm mon^{-1} in Jan. 1974 to –10.0 mm mon^{-1} in Jul. 1973. Although global average ΔPR in 1998 was trivial at the global scale (–3.55 mm yr^{-1}), regionally droughts took place in central Africa and Amazonian Basin in South America, and extra rainfalls in Monsoon Asia and Central America (cf. Fig. 5-26b). These climatic anomalies in 1998 may be interpreted in terms of the strong ENSO event which began from late 1996.

Atmospheric CO_2 concentrations increased typically from 316 ppmv in 1958 to 367 ppmv in 1998, at the average rate of +1.3 ppmv yr^{-1} (GLOBALVIEW-CO_2, 1999; Keeling and Whorf, 2000). Most of available data to date show that atmospheric CO_2 in 1998 had an extraordinary augmentation: +2.8 ppmv yr^{-1} at Crozet of the Indian Ocean (GLOBALVIEW-CO_2, 1999), +2.9 ppmv yr^{-1} at Mauna Loa (Keeling and Whorf, 2000), +3.1, +2.8, and +3.0 ppmv yr^{-1} at Yonagunijima, Minamitorishima, and Ryori in Japan, respectively (JMA, 1999).

5.5.2. Average global carbon budget

After reaching an equilibrium through the preliminary iterative calculation, global annual *GPP*, AR, *NPP*, and *HR* were estimated as 121.6, 59.6, 62.0, and 57.2 Pg C yr^{-1}, respectively. The crop harvest of 3.3 Pg C yr^{-1} and net sequestration of 1.4 Pg C yr^{-1} accounted for the equilibrium state of carbon budget. The estimation of *NPP* is adequately comparable with those of other models; Cramer et al. (1997) showed that other 16 models estimated *NPP* as 40 to 70 Pg C yr^{-1} (see Chapter 7). The global monthly *NPP* oscillated from 3.4 Pg C mon^{-1} in April to 7.6 Pg C mon^{-1} in July, the seasonality being mainly due to northern high latitudes. Global monthly *NEP* (figure not shown) was positive, i.e. uptaking carbon, during the northern growing-period (1.7 to 2.2 Pg C mon^{-1}), as reflected in the seasonal cycle of the atmospheric CO_2 concentration (e.g. Kohlmaier et al., 1987). Carbon pools in vegetation and soil organic matter were estimated as 538.4 Pg C and 1505.9 Pg C, respectively. From Table 5-3, it can be seen that the variation of carbon budget among the biomes is consistent with observations (e.g. Whittaker, 1975), from tropical rain forest (biome 1), which is productive (*NPP*: 11.0 Mg C ha^{-1} yr^{-1}) and in which carbon is abundant (C storage: 321.4 Mg C ha^{-1}), to desert (biome 11) which is the most infertile (*NPP*: 0.2 Mg C ha^{-1} yr^{-1}) and in which carbon is

scarce (C storage: 3.7 Mg C ha^{-1}).

5.5.2. Time-series of global carbon anomalies

In the NCEP/NCAR-reanalysis dataset from 1958 to 1998 (Fig. 5-5 and Table 5-4), there were warmer periods such as 1990-1991 and cooler periods such as 1975-1976, and periods with high or low precipitation. However, the global climate anomalies could not be correlated with these occurrences. In particular regions, however, they exerted notable effects on climate conditions and terrestrial carbon budget (cf. section 5.5.6).

Figures 5-8 to 5-13 show the time-series of monthly carbon flux anomalies, ΔGPP, ΔAR, ΔNPP, ΔHR, ΔNEP, and ΔNCB. It was found that considerable positive ΔNEPs broke out in 1971 and 1992, and negative one in 1983. Interestingly, the continuous anomalies in ΔAR and ΔHR for several consecutive months lead to large cumulative ΔNEPs. For example, a cumulative positive ΔNEP from Oct. 1970 to Apr. 1972 amounts to +3.80 Pg C, and negative one from Sep. 1982 to Mar. 1984 amounts to –2.66 Pg C. As with ΔNEP, the estimated time-series of annual deviations using the actual and the average climates are shown in Figs. 5-14a and 5-14b (cf. Eqs. 5-2a and 5-2b), as well as the net anomaly ΔNEP in Fig. 5-14c. In addition to Fig. 5-14c using the standard Q_{10} value of 2.0 for *ARM* and *HR*, those using different Q_{10} values, i.e. 1.5 and 2.5, are shown in Fig. 5-15, because we were aware of their importance for respirations in evaluating the carbon budget anomaly. With the Q_{10} of 2.0, the global ΔNEP fluctuated from –2.58 Pg C yr^{-1} in 1998 to +1.94 Pg C yr^{-1} in 1971 (SD=1.10 Pg C yr^{-1}), enough to have caused the observed atmospheric CO_2 anomalies. It was found, however, that a larger Q_{10} lead to larger ΔNEPs, as represented by the magnitude of standard deviation (from 0.91 Pg C yr^{-1} of Q_{10}=1.5 to 1.19 Pg C yr^{-1} of Q_{10}=2.5). Moreover, in some years, the different Q_{10} values lead to the opposite direction of anomaly: e.g. in 1974, a positive ΔNEP was estimated by Q_{10} of 2.0 and 2.5 (Figs. 5-14c and 5-15b), but a negative one by Q_{10} of 1.5 (Fig. 5-15a). Another interesting aspect in Fig. 5-14 is that the 41-year average *NEP* was estimated as a positive value (Fig. 5-15a, +1.51 Pg C yr^{-1}), implying a net carbon sequestration into the biosphere. This enhancement was obviously due to the CO_2

fertilization effect induced by the atmospheric CO_2 rise from 316.1 ppmv in 1958 to 367.3 ppmv in 1998.

Table 5-5 summarizes the specific contributions to the global ΔNEP trend, by each of the carbon fluxes and each of the four latitudinal zones (Z5 was negligible). Apparently, in the years when the biosphere had large ΔNEP: (1) both plant and soil, i.e. ΔNPP and ΔHR, acted as net carbon sinks or sources; and (2) all zones performed similarly either as sinks (e.g. 1971 and 1992) or as sources (e.g. 1973, 1983, and 1998). However, quantitatively and often qualitatively, zonal ΔNEP occurred heterogeneously rather than homogeneously across the biosphere. It can be seen from Table 5-5 that the most influential zone (values in boldface) on the global ΔNEP trend was the Z3 (i.e. tropics), which is mainly occupied by such ecologically and biogeochemically active biomes as tropical rain forest (biome 1), and which is responsible for nearly half (27.4 Pg C yr^{-1}) of global annual *NPP*. The Z3 affects global ΔNEP critically in both directions (either sink or source), in a large part of the 41-year experimental period. However, in many of the exceptional years, the biosphere was nearly neutral with respect to the carbon balance (i.e. ΔNEP<SD), and then most of the significant ΔNEP s were emanated from the Z3. The standard deviations of zonal ΔNEPs also suggest the outstanding contribution by the tropical zone Z3, such that it had by far the largest ΔNEP (±0.65 Pg C yr^{-1}) among the four zones, accounting for over half of the global total (±1.10 Pg C yr^{-1}).

5.5.4. Multiple regression analysis

Statistical analyses were conducted so as to derive some relationships between climatic anomalies (Table 5-4) and carbon flux anomalies (Table 5-5). At first, we conducted a multiple regression analysis for the three independent climatic variables, ΔTG, ΔPR and ΔRTG. Since the term ΔTG had high correlations with ΔTS_{10} and ΔTS_{200} (p<0.001), we applied it also to soil heterotrophic respiration (ΔHR). Although the precipitation (PR) itself was not used as an input of the simulation experiment, we regarded it as a plain indicator of water availability, rather than the Δ (AET/PET) ratio which would be contaminated by ΔTG.

Table 5-6 shows the standardized correlation coefficients calculated for the global biosphere and the four latitudinal zones (Z1 to Z4). In Table 5-6a, the raw coefficient values are also listed for the global analysis, which shows the responsiveness of the biospheric carbon flux to climate anomalies. Apparently, ΔAR and ΔHR had significant positive correlations with ΔTG in all regions; this leads to a high negative correlation of ΔNEP with ΔTG, globally and zonally, even during the growing-period. The highest negative correlation between ΔTG and ΔNEP (standardized correlation coefficient =–0.919, $p<0.001$) emerged in Z3, which is almost occupied by tropical evergreen forests (biome 1) and grasslands (biome 8). In these warm biomes, respirations (both *AR* and *HR*) had the highest sensitivity to temperature, as expected from the exponential dependence of both types of respiration (cf. Fig. 5-4b). On the other hand, ΔGPP and ΔNPP were less sensitive to climatic anomalies. In Z1 and Z3 (Tables 5-6c and 5-6e), ΔPR and ΔRTG had weak influence on ΔGPP and ΔNPP, while ΔTG had a moderate effect. In Z2, which contains broad areas of arid ecosystems (biomes 8, 9, and 11), higher precipitation resulted in accelerated soil decomposition (ΔHR), but little change in primary productivity (both ΔGPP and ΔNPP): thus, ΔPR and ΔNEP were negatively correlated (Table 5-6d). The sensitivity of ΔGPP and ΔNPP to ΔTG varied among the latitudinal zones, which differ in habitat temperature condition and dominant biome type correspondingly. For example, ΔGPP and ΔNPP in the cooler zone Z1 had positive correlations with ΔTG (Table 5-6c), while those in the warmer zones Z3 and Z4 had negative ones (Tables 5-6e and 5-6f).

5.5.5. Linear regression analysis

Next, we conducted a linear regression analysis to simplify and quantify the relationship between ΔTG (the most overriding factor, as shown in Table 5-6) and carbon flux anomalies; that is, $\Delta F=\beta \cdot \Delta TG$ (β is the slope of the regression line)

Annual-base. As shown in Fig. 5-16, the ΔGPP had little correlation with ΔTG (r^2=0.00, p=0.58), while the ΔAR and ΔHR had stronger correlations (r^2=0.41, $p<0.001$ and r^2=0.35, p=0.0015, respectively) and steeper slopes (β_{ann}=+1.62 and

+1.77 Pg C yr^{-1} $°C^{-1}$, respectively). The ΔNPP which is the balance of ΔGPP and ΔAR, had a moderate negative correlation with ΔTG (β_{ann}=–1.21 Pg C yr^{-1} $°C^{-1}$, r^2=0.40, p=0.0015). Since ΔNEP is the balance of ΔGPP, ΔAR, and ΔHR, it had a considerable negative correlation (r^2=0.44, p<0.001). The highest negative β_{ann} (–3.24 Pg C yr^{-1} $°C^{-1}$) between ΔTG and ΔNEP suggests that a significant amount of carbon would be immediately released from the biosphere to the atmosphere, as a result of a small global warming; a precipitation anomalies may make deviations from the regression line (Fig. 5-16e). However, Fig. 5-17 shows that tropical regions were more responsible for the strong ΔTG-ΔNEP relationship.

Monthly-base. A monthly-base analysis was also conducted: slope β_{mon} (Pg C mon^{-1} $°C^{-1}$) (Fig. 5-18). ΔGPP shows a biannual oscillation with two peaks; one is strong positive dependence on ΔTG in April and May (spring in the NH), and the other, to lesser extent in September and October (autumn), whereas virtually no dependence in July and August (mid summer in the NH) and in November to March (winter). Apparently, the substantial dependencies in spring and autumn are due to the multiple temperature effect on physiological activities and on phenological stimulation (i.e. elongation of growing-period). In summer, in contrast, because most ecosystems are largely under their thermal optima, their ΔGPPs are susceptible to neither physiological nor phenological effects of the temperature fluctuation. ΔAR had a positive slope irrespective of season; therefore, β_{mon} of ΔNPP varied almost in parallel with that of ΔGPP, i.e. positive in spring and in autumn in the NH, and negative in summer and in winter in the NH. Similarly, ΔHR had a consistently positiveβ_{mon} throughout the year. Consequently, ΔNEP had a strong negative slope exceeding –0.4 Pg C mon^{-1} $°C^{-1}$ from June to August (Fig. 5-18).

As shown in Fig. 5-19, tropical ecosystems in Z3 had negative correlations with ΔTG irrespective of seasons, whereas temperate ecosystems in Z2 and boreal ones in Z1 showed a clear seasonal change. In summer and winter, most of them had negative correlations (r<0), while in spring and autumn, these ecosystems had significantly positive ones (r>0), because a warmer temperature leads to a longer growing-period. As a result, global ΔNEP had a weaker correlation with ΔTG in spring and autumn months (e.g. r=–0.068 in April), although locally

some ecosystems had substantial responsiveness. These seasonal changes should deserve our attention in considering the impacts of climate change on the biospheric carbon budget.

5.5.6. Examples of six extreme ΔNEP years

To elucidate the underlying mechanism of large ΔNEPs, we examine features in three interesting years: the large positive ΔNEP in 1965 (+1.86 Pg C yr^{-1}), the largest positive ΔNEP in 1971 (+1.94 Pg C yr^{-1}), the large negative ΔNEP in 1973 (+2.23 Pg C yr^{-1}), the large negative ΔNEP in 1983 (–2.14 Pg C yr^{-1}), the accidental positive ΔNEP in 1992 (+1.16 Pg C yr^{-1}), and the largest negative ΔNEP in 1998 (+2.58 Pg C yr^{-1}). These years are drawn by the specific symbols in Fig. 5-16 and listed in shaded rows in Tables 5-4 and 5-5.

1965: a large positive ΔNEP and the largest negative ΔHR year

Global maps. The slightly lower temperature in 1965 (a moderate ENSO year) was ascribable to cooling in eastern Siberia and North America (Fig. 5-21). The main regions responsible for the large ΔNEP, i.e. South America and Central Africa, experienced lower precipitation (globally, ΔPR=–19.2 mm yr^{-1}).

Zonal distribution of anomalies. Around 1965 (cf. Table 5-4), apparent negative ΔTG took place in Z3 (–0.35 °C), leading to ΔNEP of +1.01 Pg C yr^{-1} mainly due to the repressed decomposition (ΔHR in Z3 was –0.55 Pg C yr^{-1}). (It is not clear whether this cooling was related to the eruption of Mt. Agung in 1963.) Both lower temperature and lower precipitation would result in the largest negative ΔHR, and then the large positive ΔNEP.

1971: the largest positive ΔNEP and ΔNPP year

Global maps. The largest positive global ΔNEP took place in 1971 (+1.94 Pg C). This is interesting as a contrast to the largest negative anomaly in 1983. In 1971, a La Niña year, eastern Pacific sea surface temperature was lower than average (Fig. 5-22a), and correspondingly global ground surface was cooler than the average by –0.20 °C (cf. Fig. 5-5). Although most tropical regions underwent moderate temperatures, they had considerable

negative ΔPR, especially in South America, Africa, and Monsoon Asia (Fig. 5-22b). Then, the distribution of carbon anomaly ΔNEP (Fig. 5-22c) seems likely to be relevant to the negative ΔPR rather than ΔTG. For example, in Africa, the distribution of ΔNEP was apparently contrastive to that of ΔPR.

Zonal distribution of anomalies. In 1971, because Z3 underwent a negative ΔTG (–0.34 °C) and a negative ΔPR (–47 mm yr^{-1}), it had the largest positive zonal ΔNEP as large as +1.11 Pg C yr^{-1} (Table 5-5). Both lower temperature and precipitation would reduce carbon emissions by respiration (ΔAR by –0.47 Pg C yr^{-1}) and decomposition (ΔHR by –0.81 Pg C yr^{-1}), as fully explained by the multiple regression analysis in section 5.3. Also note that the year 1971 had the largest positive ΔNPP by +1.25 Pg C yr^{-1}, due to both positive ΔGPP and negative ΔAR (Table 4).

1973: a large negative ΔNEP and the largest positive ΔHR year

Global maps. Ground temperature was slightly higher in 1973 (La Niña year), especially in North America and Eurasia (Fig. 5-23a). In the lower latitudinal zone, Australia and Southeast Asia experienced a moderate degree of warming. In contrast to these gentle ΔTG s, 1973 was one of the most rainy years during the experimental period (+37.3 mm yr^{-1}), especially in eastern North America, South America, southern China, and northern Australia.

Zonal distribution of anomalies. Of the global ΔNEP of –2.23 Pg C yr^{-1} in 1973, 52.9 % was from Z3 and 21.1 % was from Z4 (Table 5-5), both of which underwent higher temperature and more precipitation (Table 5-4). In other words, the largest positive ΔHR in 1973 (+1.50 Pg C yr^{-1}) may be brought about by the same mechanism to the largest negative ΔHR in 1965, but to the opposite direction. The small ΔAR in 1973 (+0.23 Pg C yr^{-1}) suggests that the predominant factor was the higher precipitation, because AR and HR had similar sensitivity to temperature. It is apparent that the South America was primarily responsible for the large ΔNEP in 1973, a La Niña year.

1983: a strong ENSO year

Global maps. Most of the climatic anomalies in 1983 may be relevant to the robust ENSO event, which began from early 1982. Accompanied with the sea surface temperature rise in eastern Pacific Ocean, coastal regions of South America had positive ΔTG (Fig. 5-24a). The positive ΔTG was also evident in Eurasian regions. From the precipitation anomaly map shown in Fig. 5-24b, we can find a larger spatial heterogeneity from positive ΔPRs in South America and part of Monsoon Asia to negative ones in Africa. Figure 5-24c shows a global distribution of ΔNEP values which were affected by ΔTG and ΔPR in 1983, where many tropical ecosystems and some temperate ecosystems in Europe and North America acted as net carbon sources, while little net carbon sequestration happened in other areas (e.g. a part of South Africa). Especially, equatorial South America which had warmer temperatures and high precipitations emitted a large amount of carbon.

Zonal distribution of anomalies. Table 5-5 shows that the carbon emission was especially evident in Z3 (–1.22 Pg C yr^{-1}), which is most sensitive to ΔTG among the four zones. In 1983, Z3 underwent a large positive ΔTG by +0.43 °C and a moderate negative ΔPR by +4.9 mm yr^{-1}. The anomalously high temperature in 1983 was particularly evident from February to July (+0.69 °C, cf. Fig. 5-6), and enhanced respiration and decomposition in the tropical ecosystems. It can be seen from Table 5-5 that Z1 and Z2 had the second largest negative ΔNEP (–0.27 and –0.49 Pg C yr^{-1}, respectively), but Z4 had the sixth largest negative ΔNEP (–0.19 Pg C yr^{-1}). These simultaneous anomalies strongly suggest the impacts of a climate perturbation at the global scale.

Biome-specific aspects. Table 5-7 summarizes such biome-specific features as climate sensitivity and contribution to global ΔNEPs. In 1983, most biomes had significantly negative ΔNEPs, especially in tropical rain forests (biome 1, –0.60 Pg C yr^{-1}) and grasslands (biome 8, –0.43 Pg C yr^{-1}). These biomes are the major component in Z3 and are sensitive to ΔTG and ΔPR (see β_{ann} in Table 5-7); a positive ΔTG (+0.3 ~ 0.4 °C) in these ecosystems would be the principal cause of the global ΔNEP. This result is consistent with the analysis by Gérard et al. (1999). However, savannas (biome 7) which were mainly occupied

with C_4 grasses exerted little effect on the global carbon budget, in spite of a large temperature anomaly (+0.5 °C).

1992: after the Mt. Pinatubo eruption

Global maps. Although annual average temperature in 1992 was lower than that in the previous year 1991 by –0.35 °C (cf. Fig. 5-25b), the temperature anomalies in 1992 (Fig. 5-25b) seem more gentle than those in 1983. Nevertheless, we can find some cooler (e.g. Middle East and northeastern North America) and warmer (e.g. Siberia and western North America) regions. As shown in Fig. 5-25c, ΔNEP values of 1992 in many ecosystems were positive, especially those in South America, North America, Monsoon Asia, and Australia. The large carbon sink in Monsoon Asia seems consistent with (maybe ENSO-induced) negative ΔPR (Fig. 5-25b) which could reduce decomposition (cf. Table 5-6).

Zonal distribution of anomalies. In 1992, the zone contributing most to global ΔNEP was Z3 (+0.40 Pg C yr^{-1}), and also Z2 had a substantial contribution (+0.36 Pg C yr^{-1}), which had a negative ΔTG (–0.30 °C) and ΔPR (–37.3 mm yr^{-1}), but no significant $\Delta PPFD_{SFC}$. The cooler temperature was especially evident from July to October (–0.85 °C in Z1, and –0.60 °C in Z2), which was certainly induced by the Mt. Pinatubo eruption in June 1991. As McCormick et al. (1995) summarized, the eruption was so robust that it gave rise to a series of chemical, optical, and climatic ramifications, leading to a global tropospheric cooling in the following few years (cf. Fig. 5-5). Additionally, $PPFD_{SFC}$ had little anomaly (cf. Fig. 5-7) in spite of the eruption, because the attenuation of direct radiation could be compensated by increased diffused solar radiation; it contains more fraction of PAR than direct radiation (Alados-Arboledas et al., 1997). Consequently, lower temperature and precipitation resulted in reduced rates of respiration (ΔAR=–0.37 Pg C yr^{-1}) and decomposition (ΔHR= –0.78 Pg C yr^{-1}).

Biome-specific aspects. In 1992, the most influential biome on ΔNEP was still the tropical evergreen forest (+0.23 Pg C yr^{-1}). Moreover, temperate deciduous forests (biome 4) and temperate and boreal needle-leaved forests (biome 5) in Z1 also made noteworthy

positive contributions (+0.21 and +0.18 Pg C yr^{-1}, respectively). Table 5-7 lists the annual global ΔTG in which cooling is not so evident, but the northern regions had larger negative ΔTG by about –0.4 °C from April to October, which include the sensitive months (cf. Fig. 5-18). Low precipitations (–29 mm yr^{-1}) that could reduce soil moisture affected ΔNEP by limiting the rate of decomposition.

1998: the largest negative ΔNEP and ΔNPP year

Overall aspects. While global land surfaces were anomalously warm from Sep. 1997 to Oct. 1998 (+0.62 °C above the mean value), monthly ΔNEP directed negative and the cumulative ΔNEP amounted to –3.0 Pg C. Especially in April 1998, the largest negative ΔNEP (as much as – 0.45 Pg C mon^{-1}) was estimated (Fig. 5-12), up to 57 % of which emanated from Z3. Compared with the southern oscillation index (SOI) showing a trough in late 1997 (NOAA, 1999), the maximum negative ΔNEP had a time-lag of three to five months behind the progress of ENSO event. After the culmination, in late 1998, ΔNEP turned from negative to positive in parallel with the termination of the ENSO event and corresponding climate trend. In sum, the most important feature in 1998 is the largest net carbon emission (as much as 2.6 Pg C yr^{-1}) which is mostly attributable to 2.3 Pg C yr^{-1} of Δ (AR+HR) and additionally 0.3 Pg C yr^{-1} of ΔGPP. Figure 5-26c shows the global map of annual ΔNEP in 1998. Nearly a half of the land areas released carbon to the atmosphere, especially from Monsoon Asia (except for inland regions), eastern Siberia, Australia, northern South America, South Africa, and eastern North America. Some severely affected ecosystems released carbon over 0.2 kg C m^{-2} yr^{-1}, or about a quarter of the average gross flux (0.85 kg C m^{-2} yr^{-1}): boreal forests in eastern Siberia, grasslands in South Africa, and tropical evergreen forests in northern South America. Most of these source regions had either warmer temperatures or more precipitations, both of which could enhance the gross carbon emission by respiration AR and decomposition HR. In contrast, ΔNEPs in North Europe were chiefly attributable to negative ΔGPPs, due to the exceptionally cooler temperature (cf. Fig. 5-26a) delaying the onset of growing-season. Latitudinally, tropical zone Z3 and northern middle

zone Z2 accounted for 45 % and 24 % of the annual global ΔNEP, respectively.

Figure 5-27 summarizes the long-term correlation between annual global ΔTG and ΔNEP, and characteristics in 1998 (cf. Fig. 5-16e). It follows that there is a close negative correlation between annual ΔTG and ΔNEP (r^2=0.436, p<0.0001); an anomalous warmth by 1 °C leads to a net carbon emission by 3.13 Pg C yr^{-1}. However, the simulated ΔNEP in 1998, –2.6 Pg C yr^{-1}, was much larger than that expected from the linear regression, i.e. –1.8 Pg C yr^{-1} resulting from +0.58 °C of ΔTG. This discrepancy would be explained by the effect of positive ΔPR on ΔHR in eastern India and northern South America, and that of negative ΔTG on ΔGPP (via shorter growing-period) in North Europe (cf. Fig. 5-26).

5.6. Discussion

5.6.1. Validity of Sim-CYCLE analysis

The multiple and linear regression analyses, shown in Figs. 5-16, 5-18, and 5-19 and Table 5-6, strongly suggest that the biospheric global carbon budget ΔNEP is sensitive to climatic anomalies, primarily in temperature and secondarily in precipitation. Since these outcomes are critically dependent on the characteristics of the simulation model used, we should carefully examine whether the sensitivity is truly due to that of the biosphere or that of Sim-CYCLE, i.e. an artifact. The formulations of carbon dynamics dependent on various environmental factors, such as Eqs. 2-39 to 2-65, are simple but would capture the physiological-scale response properly. However, there remain uncertainties about the strength of these sensitivities. Yokota and Hagihara (1996) observed that the Q_{10} value of woody plant respiration changed seasonally (i.e. larger in winter and smaller in summer), and Knorr and Heimann (1995) concluded that the most appropriate value of the Q_{10} for biospheric respiration (global AR and HR) was 1.5, rather than 2.0 (observed in situ frequently, and adopted by Sim-CYCLE). Our sensitivity analysis also suggests the importance of determining Q_{10} values in appraising the CO_2 budget, and the results using Q_{10}=1.5 may indicate the lower end of biospheric response, and those using Q_{10}=2.5 the higher end.

The following facts may, however, allow us to confirm the credence of the model

analyses presented in this paper: (1) Sim-CYCLE well simulated the features of the contemporary terrestrial carbon budget; and (2) our model analyses agreed satisfactorily with the estimation of ΔNEP derived from analyses of atmospheric CO_2 and its stable carbon isotope (Keeling et al., 1995; Joos et al., 1999). In fact, the simulated monthly ΔNEP trend agrees with one by Keeling et al. (1995) (dotted line in Fig. 5-28a), who estimated the net terrestrial and ocean carbon exchanges based on the anomalies in the atmospheric CO_2 concentration and its stable carbon isotopic composition. For example, in 1983 and 1988, when they suggested large net terrestrial emissions, Sim-CYCLE also estimated negative ΔNEPs of comparable magnitude (i.e. 0.2 Pg C mon^{-1}). On the other hand, in 1985, 1989, and 1992, when they suggested net sequestrations, Sim-CYCLE also estimated positive ΔNEPs.

A point-to-point test is desirable and effective to validate the model analysis, at the ecosystem scale. Using the eddy-correlation method, many researchers have measured net ecosystem energy and gas fluxes under various field conditions (e.g. Goulden et al., 1996). They show that the carbon balance of terrestrial ecosystems has a substantial interannual variation greater than 1 Mg C ha^{-1} yr^{-1} (potentially a few Pg C yr^{-1} at the global scale) reflecting the change in habitat weather conditions (Yamamoto et al., 1999). Although a direct comparison was not carried out, we expect that there is a semi-quantitative agreement between these measurements and our model analysis. Another interesting fact is that these flux-oriented studies often suggest that the observed ecosystems are working as a net carbon sink. Including the CO_2 fertilization effect, the Sim-CYCLE simulation also implied a net carbon sequestration into the biosphere (+1.35 Pg C yr^{-1}), of a magnitude comparable to the assumed missing sink.

5.6.2. Mechanisms of the large ΔNEP

The Sim-CYCLE analysis could account in part for the anomalously high growth rate of the atmospheric CO_2 concentration after the outbreak of ENSO events (Bacastow, 1976; Keeling et al., 1989). Probably, the effect of ENSO is considerably relevant to the largest ΔNEP in the tropical zone Z3 (cf. Table 5-6). The dominant effect of the Z3 on the

ineterannual change is remarkable, because the Z3 shows a merely small seasonal change in monthly *NEP*. After the ENSO episodes in 1983 and 1987, Sim-CYCLE estimated larger carbon emissions from the biosphere (see Fig. 5-14), and conversely in 1989 after La Niña it estimated larger carbon uptakes, so that the atmospheric CO_2 had corresponding anomalies. However, there remain uncertainties with respect to the effect of ENSO events on ecosystem carbon budget. For example, the Sim-CYCLE analysis does not account for the observed time-lags in the atmospheric CO_2, behind the anomalies in air temperature (Keeling et al., 1989) and in Southern Oscillation Index (Bacastow, 1976; Rayner et al., 1999). Because of the time-lag, most of the impacts of the huge ENSO event in 1997 would emerge in 1998 not included here. The CO_2 anomaly in relation to the ENSO events would essentially include oceanic processes, such as the interruption of the upwelling of CO_2-rich deep water (Dettinger and Ghil, 1998; Feely et al., 1999); the oceanic carbon budget has a comparative variability (SD=±1.0 Pg C yr^{-1}; Joos and Bruno, 1998) to the terrestrial one (SD=±1.10 Pg C yr^{-1}, see Table 5-5). In sum, the terrestrial mechanism had a partial contribution to the observed CO_2 anomaly, but determining its magnitude requires more information and research. Although apparent correspondence between ENSO indices and atmospheric CO_2 growth rate has already been pointed out (Bacastow, 1976; Keeling et al., 1989), the mechanism provoking the oceanic and terrestrial carbon anomalies remains unclear. The oceanic process, i.e. weakened upwelling of deep-water, is most likely (Francey et al., 1995; Feeley et al., 1999), while the terrestrial role is an open question (Kaduk and Heimann, 1994; Braswell, et al., 1997; Rayner et al., 1999). In our long-term simulation (cf. Fig. 5-12), strong ENSO events tend to coincide with negative ΔNEPs; for example, at the ENSO event in 1983, higher temperatures (+0.23 °C) and excess precipitations (+23.4 mm yr^{-1}) resulted in a net carbon emission by 2.2 Pg C yr^{-1}. Although our simulation analysis did not include the effect of biomass burning which could amplify ΔNEP in tropical regions during the ENSO-induced droughts, we would conclude that the simulated large carbon emission may be responsible, at least in part, for the accelerated growth rate of atmospheric CO_2 concentration in 1998; –2.7 Pg C yr^{-1} is equivalent to +1.26 ppmv yr^{-1}.

In relation to the Pinatubo carbon anomaly, it was hypothesized that the large ΔNEP in 1992 (+1.16 Pg C yr^{-1}) was brought about by a series of causal relationships since the Mt. Pinatubo eruption in June 1991 (McCormick et al., 1995; Jones and Kelly, 1996; Alados-Alboledas et al., 1997). The estimated ΔNEP in 1992 agrees satisfactorily with the atmospheric CO_2-based value (i.e. +1.0 to 2.5 Pg C yr^{-1} by Keeling et al., 1995), although a contradictory estimation was presented by Francey et al. (1995). We acknowledge indeed that the Pinatubo carbon anomaly was not a simple phenomenon as hypothesized here, because the oceanic processes might be induced as suggested by Sarmient (1993). Nevertheless, there are several lines of sound evidence supporting the conclusion that the biospheric processes should make a substantial contribution to the anomaly in the atmospheric CO_2 concentration. For example, Ciais et al. (1995) also estimated a net carbon uptake in the northern middle to high latitudinal ecosystems in 1992 using the SiB2 model, but their estimation (+3.5 Pg C) is much larger than ours (+0.59 Pg C, in Z1 and Z2).

5.6.3. Caveats

On the role of the terrestrial biosphere in the interannual carbon budget, there are several caveats demanding further considerations and modifications to the modelling research, including our analysis. Since Dai and Fung (1993) and Kaduk and Heimann (1994) studied the annual carbon budget of terrestrial ecosystems with empirical models, the issue has attracted the attentions of modelers. For example, Kindermann et al. (1996) applied the Frankfurt Biosphere Model to interannual change from 1980 to 1992, and they found similar features as described in this paper. However, they ascribed the interannual change in ΔNEP mainly to that of ΔNPP rather than ΔHR. Myneni et al. (1997) analyzed the temporal change in remotely-sensed NDVI, and showed that the biospheric carbon budget is sensitive to the interannual change in temperature. They concluded that warmer climate during recent years leads to a prolonged growing-period of vegetation and consequently an increased production. Our model analysis is nearly coincident with their satellite-based analysis; e.g. in 1983 negative anomalies were estimated in both observed NDVI and model-based *NPP*. However,

we can not account for the significantly positive anomalies in NDVI in 1989 to 1990, when Sim-CYCLE estimated little ΔNPP. Braswell et al. (1997) analyzed the correspondence between ΔNEP and ΔTG, and suggested a response time-lag of approximately two years. Although they attributed the time-lag to an undetermined underground process, we did not find out the nature of the process in this paper, in which responses at the physiological level were mainly addressed. Applying a process-based model (Terrestrial Ecosystem Model), Tian et al. (1998) simulated the carbon budget of the Amazon Basin from 1980 to 1994, and suggest that the regional ΔNEP varied substantially during this period, and that it was sensitive to temperature and soil water change. In sum, the model analysis presented in this paper is one of a few studies that analyzed the interannual time-series of carbon budget anomalies with a mechanistic model and accurate climate dataset.

The climate sensitivity of the biospheric carbon budget may have an important implication with respect to the impact of anticipated global change (IPCC, 1996). According to the estimated negative ΔTG-ΔNEP relationship (Fig. 5-16e), global warming is likely to lead to net release of carbon, i.e. the biotic positive feedback to the prescribed warming, at least at the short-term. However, our model analyses revealed that the ΔTG-ΔNEP relationship changes zonally (Table 5-6) and seasonally (Figs. 5-18 and 5-19), and that the precipitation anomaly could play an important role in the carbon budget in northern high and middle latitude zones (Table 5-6). Explicitly, our result suggests that we should develop a finer model and perform a series of sensitivity analyses, so that we are able to quantify the feedback effect. For example, Sim-CYCLE does not yet contain the nutrient dynamics in the soil, which may have a close linkage with carbon dynamics and also be sensitive to temperature (McGuire et al., 1997). In addition, since we focused on the effects of climatic perturbations in this study, the biospheric carbon budget was assumed to be at equilibrium at the beginning of the simulation. Then, the additional human land-use change after 1970 and the carbon emission accompanied with deforestation were not included. In the strong ENSO events in 1982-83 and 1997-98, broad areas of tropical forests in Southeast Asia suffered from fire due to drought promoting biomass inflammability. However, we know little about how

much carbon was lost from the burned forests, and how much was restored by the following successional regrowth. As Schimel et al. (1997) stated, we should take care that disturbance processes (both natural and anthropogenic) are essential parts of ecosystem dynamics and biogeochemistry, especially when we appraise the biotic feedbacks under the future global change. An improved model and simulation result covering a longer term will be presented by our forthcoming research.

Table 5-1. Biome types used for the model analysis, and their area and frequency in the T62 Gaussian grid scale. Original data are after Matthews et al. (1983) including the potential biome and the cultivation intensity for each grid point. Areas of natural vegetation are listed in five latitudinal zones (Z1 to Z5). Figures in boldface indicate the distribution center that has the largest area for each biome. Underlined figures indicate the most dominant biome for each latitudinal zone.

		Z1	Z2	Z3	Z4	Z5	Total		
		90-50°N	50-20°N	20°N-20°S	20-50°S	50-90°S	Natural	Cultivated	Frequency
	Biome	(10^6 km^2)							(cells)
1	Tropical evergreen forest	0.0	0.0	**11.9**	0.4	0.0	12.3	0.3	287
2	Tropical seasonal forest	0.0	**3.2**	2.4	1.2	0.0	6.8	1.9	211
3	Temperate broad-leaved evergreen forest	0.0	**1.0**	0.0	0.4	0.0	1.4	0.5	51
4	Temperate deciduous forest	**7.9**	1.9	0.0	0.0	0.0	9.8	4.1	526
5	Temperate and boreal needle-leaved forest	**5.5**	4.6	0.6	0.5	0.1	11.2	0.5	424
6	Woodland	**4.3**	0.7	1.5	0.9	0.0	7.5	0.4	318
7	Savanna	0.0	0.2	**3.8**	0.1	0.0	4.0	1.0	117
8	Grassland	2.1	9.4	**10.4**	**5.4**	0.1	27.3	6.2	918
9	Shrub	0.7	**5.3**	1.9	4.0	0.1	12.0	0.8	367
10	Tundra	**6.5**	0.0	0.0	0.0	0.0	6.5	0.0	370
11	Desert	0.3	**11.5**	1.6	1.1	0.0	14.5	0.3	401
12	Ice sheet	2.4	0.0	0.0	0.0	**12.1**	14.5	0.0	1838
	Land total	29.8	37.7	34.0	13.9	12.4	127.7	16.0	5828

Table 5-2. Ecophysiological parameters in Sim-CYCLE.

Biome*	PC_{MAX}	KA	T_{MIN}	T_{OPT}	T_{MAX}	GS_{MAX}	KM_{GS}	$SARM_{(TG=15℃)}$			$SHR_{(TS=15℃)}$	
								leaf	stem	root	litter	humus
1	23	0.60	3	25	45	200	30	0.25	0.019	0.065	0.047	0.025
2	25	0.60	3	25	45	200	25	0.23	0.009	0.042	0.043	0.031
3	18	0.55	0	22	38	190	30	0.34	0.022	0.085	0.042	0.026
4	21	0.50	-1	20	38	190	30	0.31	0.019	0.045	0.047	0.026
5	21	0.50	-4	20	38	190	30	0.30	0.008	0.025	0.049	0.032
6	21	0.48	-4	22	42	150	20	0.44	0.034	0.270	0.040	0.031
7 C_3	19	0.47	-2	25	45	140	20	0.52	0.062	0.340	0.037	0.028
C_4	28	0.44	6	35	55	210	20	0.56	0.230	0.440	0.037	0.028
8 C_3	19	0.45	-2	22	45	140	20	0.53	0.068	0.340	0.042	0.031
C_4	30	0.43	6	34	55	230	20	0.56	0.230	0.440	0.042	0.031
9	20	0.51	-2	25	45	140	20	0.51	0.025	0.290	0.038	0.032
10	19	0.47	-5	20	40	180	30	0.32	0.034	0.290	0.027	0.012
11	19	0.48	-3	26	44	150	15	0.50	0.059	0.270	0.063	0.055
cult.	24	0.48	-3	23	42	200	20	0.29	0.050	0.220	0.050	0.037

PC_{MAX}, maximum photosynthetic rate (μ mol CO_2 m^{-2} s^{-1}); KA, light attenuation coefficient (dimensionless);
T_{MIN}, T_{OPT}, and T_{MAX}, minimum, optimum, and maximum temperatures for photosynthesis, respectively (℃);
GS_{MAX}, maximum stomatal conductance (mmol CO_2 m^{-2} s^{-1}); KM_{GS}, coefficient of stomatal conductance (mmol CO_2 m^{-2} s^{-1});
$SARM_{(TG=15℃)}$, specific maintenance respiration rate for each organ at 15 ℃ (Mg C Mg C^{-1} day^{-1}); and $SHR_{(TS=15℃)}$, specific heterotrophic respiration rate for each soil compartment at 15 ℃ soil temperature (Mg C Mg C^{-1} day^{-1}).

Table 5-3. Average climatic conditions and estimated carbon budget for each biome.

Biome*		Climatic condition: *TG* (℃) AV	*TG* (℃) SD	*PR* (mm yr^{-1}) AV	*PR* (mm yr^{-1}) SD	*SWR* (W m^{-2}) AV	*SWR* (W m^{-2}) SD	*NPP* (Mg C ha^{-1} yr^{-1}) AV	*NPP* (Mg C ha^{-1} yr^{-1}) SD	C mass (Mg C ha^{-1}) AV	C mass (Mg C ha^{-1}) SD
1	(Z3)	23.1	2.6	2489	1032	223	19	11.0	1.1	321	85
2	(Z2)	20.7	5.6	1683	757	240	18	7.7	1.0	235	66
3	(Z2)	14.1	3.4	1443	695	211	19	8.0	2.5	328	116
4	(Z1)	6.3	9.4	821	375	170	26	6.5	2.9	314	158
5	(Z1)	-0.2	3.8	721	250	199	34	5.5	1.7	346	99
6	(Z1)	4.1	15.1	782	580	195	54	3.3	4.2	102	143
7	(Z3)	22.4	2.5	1006	506	263	15	6.0	1.9	134	56
8	(Z3)	14.9	10.4	721	677	246	35	4.4	3.4	104	86
9	(Z2)	15.2	8.7	300	415	252	36	3.8	3.8	144	152
10	(Z1)	-9.9	4.8	365	212	146	12	1.2	2.1	147	228
11	(Z2)	18.8	11.2	71	125	287	30	0.2	0.6	4	13
12	(Z5)	-34.6	13.0	147	240	158	10	0.0	0.0	0	0
cult.		14.3	8.0	904	614	229	32	4.9	1.1	74	35

*latitudinal zone in which each biome mainly distributes is in parenthesis

Table 5-4. Climate anomalies derived from the NCEP/NCAR-reanalaysis data. Zonal values are also listed for ΔTG. Exemplified years in text, i.e. 1965, 1971, 1973, 1983, 1992, and 1998 are in shaded rows.

	ΔPR	ΔSWR	ΔTG				
	(mm y^{r-1})	(W m^{-2})	(℃)				
Year			Global	Z1	Z2	Z3	Z4
1958	28.5	-3.51	0.19	0.03	0.52	0.15	0.34
1959	30.2	-2.86	0.08	0.19	0.24	0.01	0.23
1960	16.9	-2.29	-0.08	-0.16	0.31	-0.14	-0.11
1961	19.8	-2.10	-0.02	-0.02	0.14	-0.31	0.32
1962	4.2	-1.87	-0.07	0.12	0.17	-0.27	-0.09
1963	-1.1	-2.22	-0.02	0.00	0.28	-0.26	0.14
1964	-4.1	-1.98	-0.24	-0.31	0.01	-0.36	-0.27
1965	-19.2	-1.40	-0.15	-0.45	0.25	-0.35	0.06
1966	-11.4	-1.94	-0.10	-0.60	0.48	-0.12	-0.26
1967	-27.9	-0.29	-0.08	0.20	-0.14	-0.25	0.02
1968	-44.9	0.70	-0.21	-0.22	-0.09	-0.21	-0.16
1969	-38.5	0.85	-0.14	-0.92	0.16	0.32	0.14
1970	-24.3	1.22	-0.03	-0.31	0.16	0.11	-0.21
1971	-20.5	0.89	-0.20	-0.10	-0.24	-0.30	-0.39
1972	-26.7	0.44	-0.33	-0.93	-0.45	-0.02	-0.06
1973	37.3	-0.51	0.11	0.23	-0.10	0.22	0.25
1974	23.9	-0.46	-0.47	-0.70	-0.56	-0.39	-0.41
1975	30.7	-0.15	-0.14	0.36	-0.36	-0.28	-0.20
1976	3.2	-0.31	-0.48	-0.59	-0.53	-0.32	-0.68
1977	7.7	0.93	0.00	0.04	0.07	-0.12	0.05
1978	4.8	1.27	-0.18	-0.35	-0.27	-0.06	-0.13
1979	-3.6	0.09	-0.06	-0.38	0.09	0.16	0.22
1980	-16.1	1.09	0.26	0.13	0.02	0.28	0.28
1981	1.9	0.74	0.31	1.01	0.05	-0.01	-0.17
1982	-6.3	0.61	-0.12	-0.25	-0.12	0.10	0.07
1983	21.4	0.70	0.22	0.59	-0.08	0.43	0.14
1984	34.6	0.77	-0.15	-0.22	-0.45	0.00	-0.10
1985	17.3	0.52	-0.07	-0.22	-0.13	-0.05	0.19
1986	11.9	0.83	0.06	0.15	-0.07	-0.03	0.19
1987	5.6	1.25	0.17	-0.17	0.23	0.44	0.12
1988	13.0	0.98	0.36	0.62	0.16	0.26	0.12
1989	12.7	1.28	0.05	0.52	-0.10	-0.14	-0.11
1990	15.8	0.13	0.39	0.44	0.41	0.27	0.17
1991	1.0	0.51	0.38	0.51	0.10	0.27	0.31
1992	-22.7	0.79	-0.05	0.05	-0.30	0.06	-0.20
1993	-2.1	0.61	-0.15	0.09	-0.31	0.02	0.05
1994	-33.1	1.90	-0.03	-0.01	0.08	-0.12	-0.18
1995	-13.1	0.81	0.28	0.92	0.05	0.22	0.00
1996	-16.6	1.24	-0.04	-0.25	-0.15	0.01	-0.10
1997	-4.7	0.47	0.15	0.49	-0.03	0.14	0.16
1998	-5.5	0.25	0.58	0.46	0.53	0.63	0.27
SD	20.7	1.33	0.23	0.45	0.27	0.25	0.23

Table 5-5. Estimated annual global carbon flux anomalies, in case of Q_{10}=2.0. Zonal values are also listed for ΔNEP. Exemplified years in text, i.e. 1965, 1971, 1973, 1983, 1992, and 1998 are in shaded rows. Maximum and minimum in each column are given in bold.

	Annual carbon flux anomaly (Pg C yr^{-1})									
	ΔGPP	ΔAR	ΔNPP	ΔHR	ΔNCB	ΔNEP				
Year						Global	Z1	Z2	Z3	Z4
1958	0.63	0.77	-0.14	0.98	-1.12	-1.12	0.15	-0.06	-0.72	**-0.50**
1959	-0.40	-0.22	-0.17	0.76	-0.89	-0.93	-0.09	-0.18	-0.30	-0.36
1960	-0.72	-0.54	-0.18	-0.19	0.02	0.01	-0.08	0.18	-0.08	-0.01
1961	-0.79	-0.56	-0.24	-0.03	-0.20	-0.20	-0.08	0.00	0.03	-0.15
1962	-0.90	-0.86	-0.04	-0.55	0.49	0.51	0.12	0.30	-0.10	0.18
1963	-0.52	-0.47	-0.04	-0.33	0.28	0.28	0.00	0.25	0.21	-0.18
1964	**-0.92**	-1.13	0.22	-0.89	1.09	1.10	0.08	0.27	0.48	0.27
1965	0.14	-0.51	0.66	**-1.20**	1.80	1.86	0.20	0.48	1.01	0.16
1966	0.80	0.05	0.75	-0.45	1.17	1.20	0.24	0.44	0.36	0.16
1967	0.53	-0.03	0.55	-0.49	0.99	1.04	0.13	0.41	0.64	-0.15
1968	0.62	-0.02	0.64	-0.88	1.50	1.52	0.13	0.36	1.10	-0.06
1969	0.34	0.95	-0.61	-0.40	-0.18	-0.21	-0.05	0.19	-0.39	0.04
1970	0.46	0.42	0.04	-0.26	0.31	0.31	-0.07	0.23	-0.11	0.25
1971	0.66	-0.47	**1.13**	-0.81	**1.87**	**1.94**	0.06	**0.54**	**1.11**	0.22
1972	0.62	0.37	0.25	-0.59	0.82	0.85	-0.10	0.32	0.46	0.17
1973	-0.49	0.23	-0.73	**1.50**	-2.21	-2.23	-0.25	-0.32	-1.18	-0.47
1974	-0.53	**-1.18**	0.65	-0.10	0.72	0.75	-0.27	0.34	0.79	-0.10
1975	0.09	-0.38	0.47	0.36	0.10	0.11	-0.25	-0.10	0.29	0.19
1976	-0.34	-0.84	0.50	-0.57	1.01	1.06	-0.22	0.36	0.62	0.31
1977	0.64	0.47	0.18	0.27	-0.10	-0.09	-0.02	-0.19	0.17	-0.05
1978	-0.46	-0.12	-0.35	-0.06	-0.27	-0.29	-0.13	-0.14	-0.13	0.10
1979	0.20	0.52	-0.31	0.98	-1.33	-1.30	-0.10	-0.03	-1.09	-0.08
1980	-0.78	0.25	-1.02	0.31	-1.24	-1.33	-0.16	-0.27	-0.79	-0.10
1981	-0.57	-0.26	-0.32	0.45	-0.73	-0.76	**-0.30**	-0.31	-0.29	0.15
1982	-0.23	0.13	-0.36	0.50	-0.87	-0.87	-0.01	-0.31	-0.64	0.10
1983	-0.22	0.60	-0.82	1.32	-2.09	-2.14	-0.27	-0.46	**-1.22**	-0.19
1984	-0.60	-0.64	0.04	0.46	-0.41	-0.41	0.02	-0.08	-0.24	-0.12
1985	-0.39	-0.31	-0.08	-0.05	-0.01	-0.02	0.07	-0.28	0.26	-0.07
1986	0.20	-0.02	0.22	0.20	0.02	0.02	0.04	-0.23	0.31	-0.10
1987	0.42	0.90	-0.48	0.64	-1.07	-1.12	0.05	-0.36	-0.78	-0.03
1988	-0.09	0.35	-0.43	0.72	-1.12	-1.16	-0.16	-0.40	-0.63	0.04
1989	0.30	-0.31	0.61	0.05	0.53	0.57	0.04	-0.02	0.45	0.09
1990	0.57	0.70	-0.13	0.57	-0.68	-0.70	0.18	-0.35	-0.51	-0.03
1991	0.11	0.31	-0.20	0.34	-0.47	-0.54	0.19	-0.38	-0.42	0.07
1992	0.01	-0.37	0.38	-0.78	1.13	1.16	0.27	0.36	0.40	0.14
1993	0.22	-0.09	0.31	-0.66	0.98	0.97	0.16	0.19	0.50	0.12
1994	**0.86**	0.29	0.57	-0.73	1.28	1.30	**0.28**	-0.18	0.85	**0.34**
1995	0.65	0.66	-0.01	-0.04	0.02	0.03	0.17	-0.05	-0.30	0.21
1996	-0.40	-0.35	-0.05	-1.00	0.93	0.95	0.07	0.16	0.49	0.22
1997	0.56	0.51	0.05	-0.43	0.43	0.48	0.16	0.04	0.60	-0.33
1998	-0.29	**1.21**	**-1.51**	1.08	**-2.49**	**-2.58**	-0.20	**-0.71**	-1.18	-0.48
SD	0.53	0.57	0.52	0.68	1.07	1.10	0.16	0.31	0.65	0.21

Table 5-6. Standard correlation coefficients between the anomalies in carbon fluxes and the anomalies in climatic factors: surface temperature (ΔTG), precipitation (ΔPR), and irradiance (ΔSWR). To offset the scale difference among the climatic factors, standardized correlation coefficients are listed (**, $p<0.001$; *, $p<0.01$), except for the global one (A), which lists the raw correlation coefficients. Note that *TG* and *SWR* are the model input data, but *PR* is not.

(A) Global / raw (Pg C yr^{-1})

	ΔTG (°C)	ΔPR(mm)	ΔSWR (W m^{-2})
ΔGPP	0.359	-0.013	-0.066
ΔAR	1.553	-0.009	-0.079
ΔNPP	-1.194	-0.004	0.013
ΔHR	1.529	0.018	-0.119
ΔNEP	-2.646	-0.022	0.146

(B) Global / standardized

	ΔTG	*ΔPR*	*ΔSWR*	r^2
ΔGPP	0.161	-0.516	-0.075	0.146
ΔAR	0.721**	-0.355	-0.093	0.500
ΔNPP	-0.564*	-0.181	0.016	0.284
ΔHR	0.557**	0.576**	-0.110	0.702
ΔNEP	-0.602**	-0.435*	0.085	0.561

(C) Z1 (N. High) / standardized

	ΔTG	*ΔPR*	*ΔSWR*	r^2
ΔGPP	0.654**	-0.368	-0.245	0.541
ΔAR	0.715**	-0.408	-0.142	0.613
ΔNPP	0.594*	-0.329	-0.306	0.473
ΔHR	0.689**	0.320	-0.089	0.667
ΔNEP	-0.055	-0.755*	-0.277	0.282

(D) Z2 (N.Middle) / standardized

	ΔTG	*ΔPR*	*ΔSWR*	r^2
ΔGPP	0.476	-0.188	-0.495	0.212
ΔAR	0.843**	-0.100	-0.085	0.630
ΔNPP	-0.172	-0.143	-0.548	0.262
ΔHR	0.538**	0.526**	0.186	0.577
ΔNEP	-0.475*	-0.481*	-0.402	0.560

(E) Z3 (Tropical) / standardized

	ΔTG	*ΔPR*	*ΔSWR*	r^2
ΔGPP	-0.367	-0.399	0.311	0.416
ΔAR	0.684**	-0.360	0.012	0.626
ΔNPP	-0.993**	-0.021	0.274*	0.923
ΔHR	0.717**	0.291	-0.359	0.667
ΔNEP	-0.919**	-0.160	0.336*	0.858

(F) Z4 (S.Middle) / standardized

	ΔTG	*ΔPR*	*ΔSWR*	r^2
ΔGPP	-0.377	-0.476	-0.136	0.142
ΔAR	0.437	-0.252	0.067	0.232
ΔNPP	-0.871**	-0.371	-0.233	0.699
ΔHR	0.338*	0.580*	-0.276	0.683
ΔNEP	-0.716**	-0.593*	0.054	0.771

Table 5-7. Biome-specific features in 1983 and 1992: $\triangle TG$, $\triangle PR$, and $\triangle NEP$, in case of Q_{10}=2.0.

	β ann (slope of regression)		1983 (robust ENSO year)				1992 (post-Mt.Pinatubo-eruption year)			
	ΔTG - ΔNEP	ΔPR - ΔNEP	$\triangle TG$ *1	$\triangle PR$ *1	$\triangle NEP$		$\triangle TG$ *1	$\triangle PR$ *1	$\triangle NEP$	
Biome*2	(Mg C ha^{-1} yr^{-1} °C^{-1})	(Mg C ha^{-1} yr^{-1} 100mm^{-1})	(°C)	(mm yr^{-1})	(Mg C ha^{-1} yr^{-1})	(Pg C yr^{-1})	(°C)	(mm yr^{-1})	(Mg C ha^{-1} yr^{-1})	(Pg C yr^{-1})
1 (Z3)	-1.31	-0.10	0.41	9.1	-0.50	-0.61	0.00	-1.5	0.22	0.27
2 (Z2)	-0.71	-0.15	0.09	77.2	-0.26	-0.17	-0.13	-127.3	0.21	0.14
3 (Z2)	-0.27	-0.13	0.07	73.3	-0.24	-0.03	-0.32	-54.0	0.29	0.04
4 (Z1)	-0.27	-0.19	0.68	59.1	-0.12	-0.14	0.16	-77.3	0.20	0.22
5 (Z1)	0.01	-0.23	0.46	67.2	-0.19	-0.18	0.23	-57.5	0.18	0.17
6 (Z1)	-0.16	-0.06	0.41	-31.6	-0.19	-0.14	-0.12	-1.2	0.06	0.05
7 (Z3)	-0.36	-0.14	0.51	-43.5	-0.04	-0.02	0.31	-16.5	-0.14	-0.06
8 (Z3)	-0.27	-0.16	0.32	12.5	-0.18	-0.49	-0.05	-29.6	0.07	0.20
9 (Z2)	-0.17	-0.15	0.26	33.2	-0.07	-0.09	-0.22	19.0	0.00	0.00
10 (Z1)	0.00	0.02	0.09	-2.5	-0.04	-0.02	-0.44	-16.1	0.03	0.02
11 (Z2)	0.00	-0.01	-0.15	-1.6	0.00	-0.002	-0.42	5.3	0.00	-0.007
cult.	-0.18	-0.09	0.26	28.8	-0.10	-0.15	0.01	-48.2	0.07	0.11
Total*3	-0.27	-0.20	0.30	22.4	-0.16	-2.06	-0.07	-29.1	0.09	1.14

*1 long-term mean conditions are listed in Table 5-3.

*2 latitudinal zone in which each biome mainly distributes is in parenthesis

*3 area-weighted average except ice sheet (biome 12)

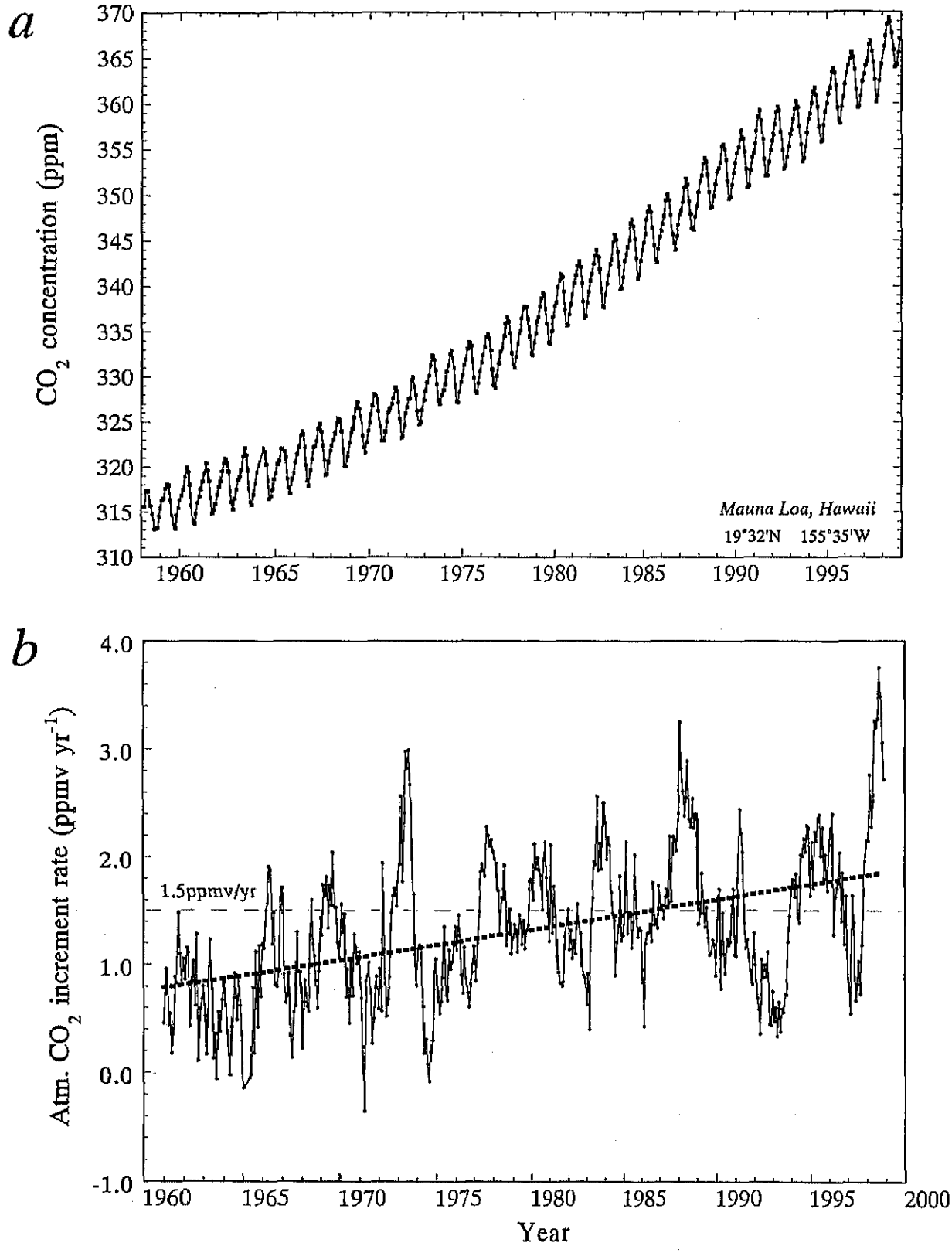

Fig. 5-1. Observed time-series of atmospheric CO_2 concentration, at Mauna Loa, Hawaii (after Keeling and Whorf, 1999). (a) Monthly mean concentration, and (b) its growth rate.

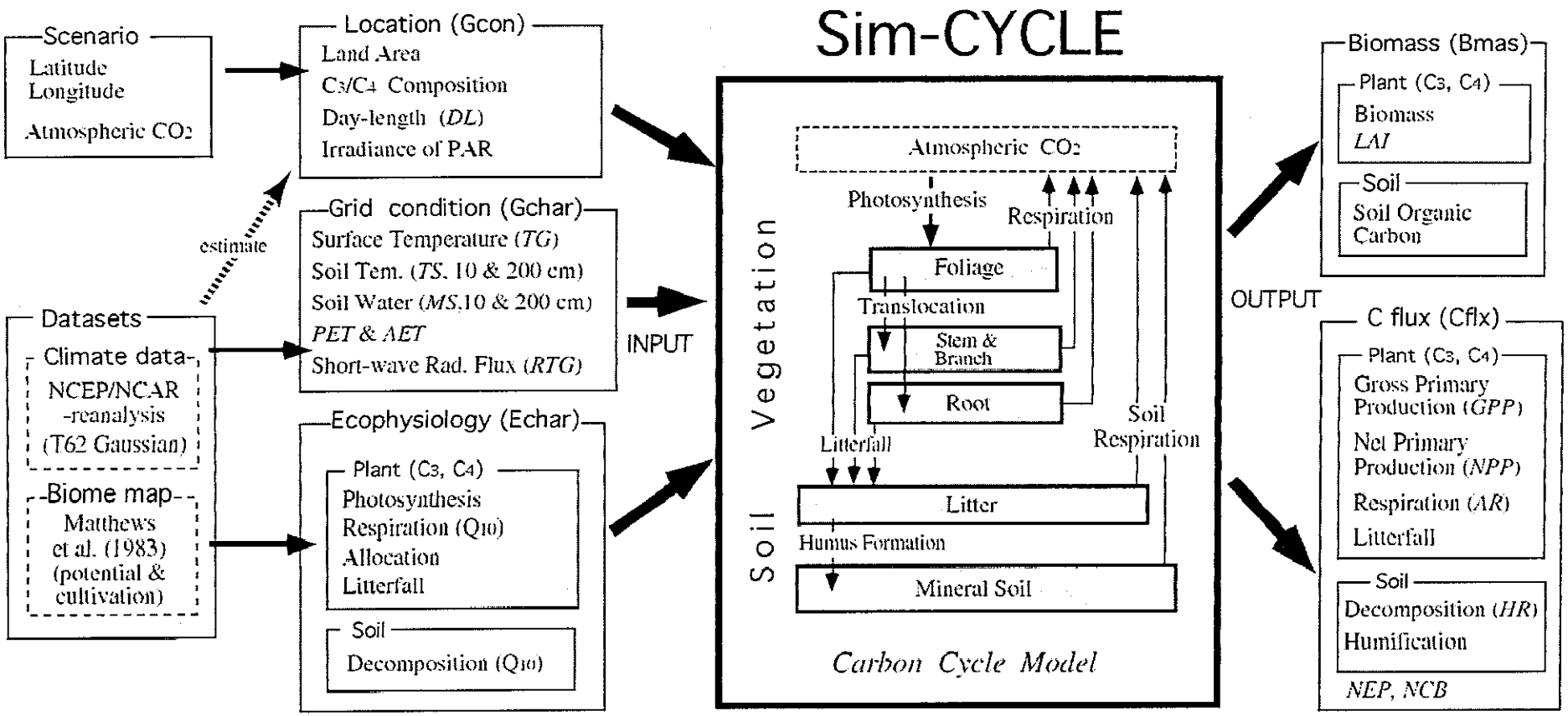

Fig. 5-2. Schematic diagram of the Sim-CYCLE 41-year analysis, using the NCEP/NCAR-reanalysis data, from 1958 to 1998.

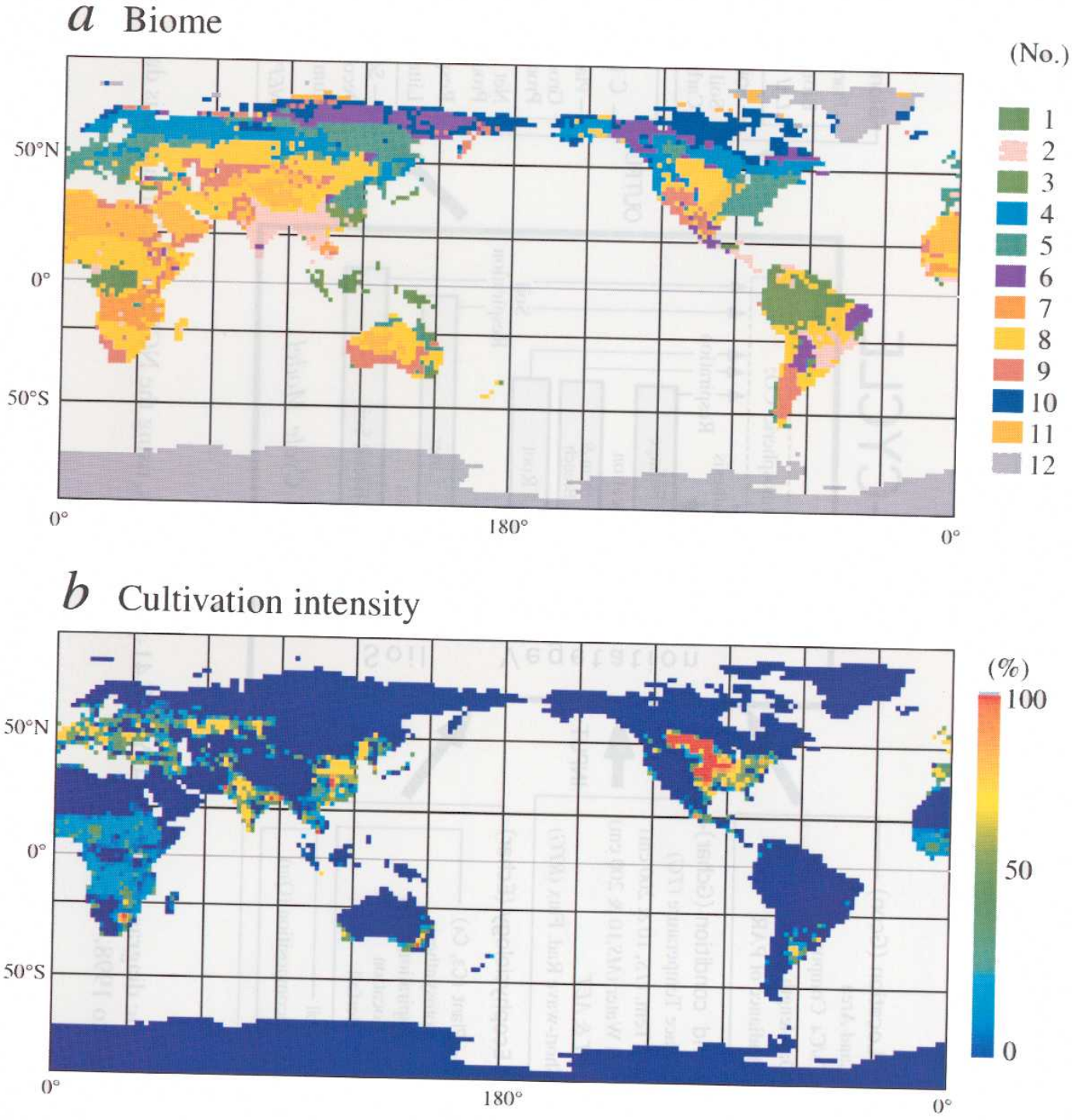

Fig. 5-3. Land cover condition in Sim-CYCLE 41-year run. (a) Biome distribution, and (b) cultivation intensity. Data from Matthews et al. (1983). Spatial resolution was adjusted to T62 (5,862 land cells).

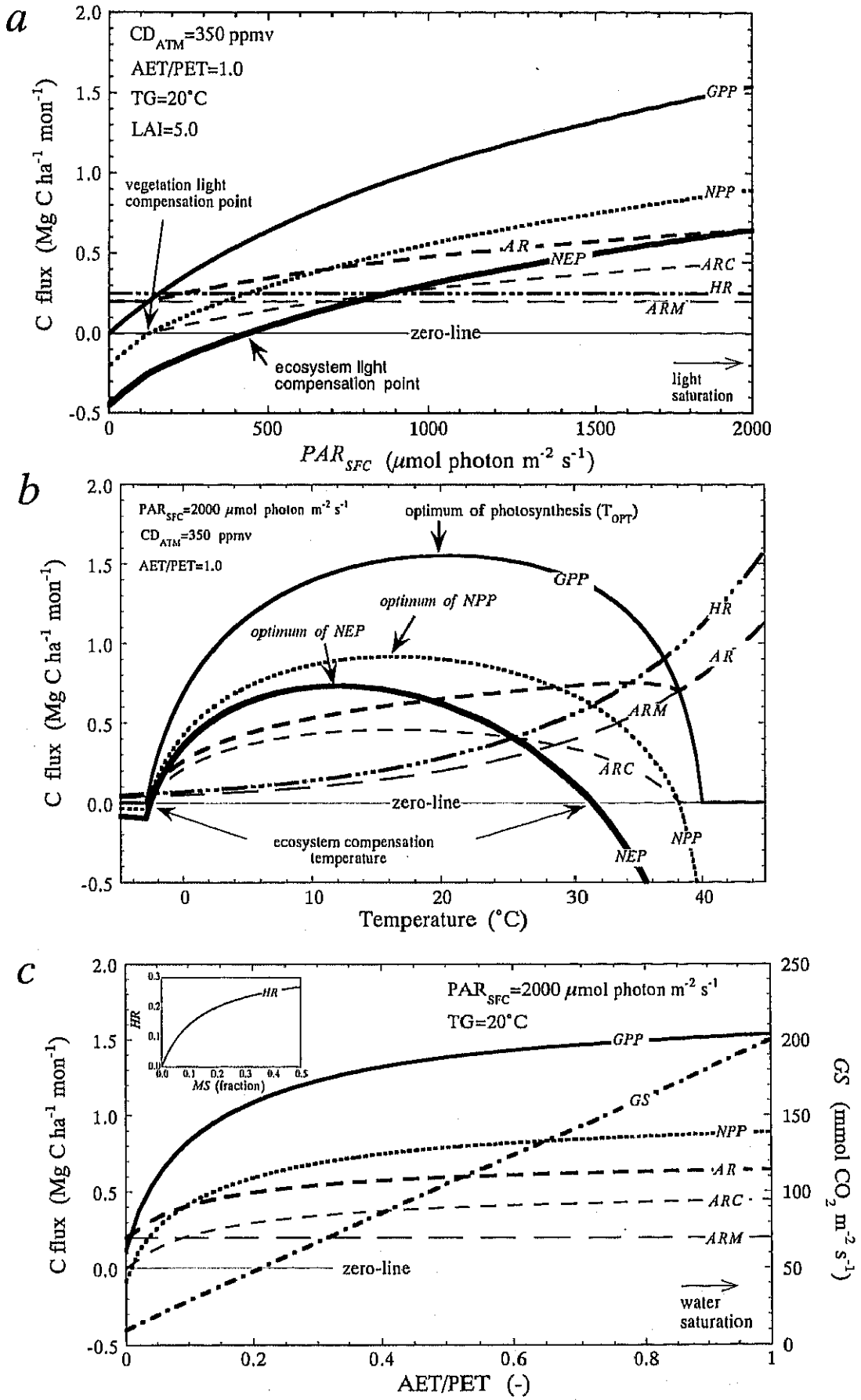

Fig. 5-4. Dependencies of carbon fluxes on (a) light, (b) temperature, and (c) water conditions.

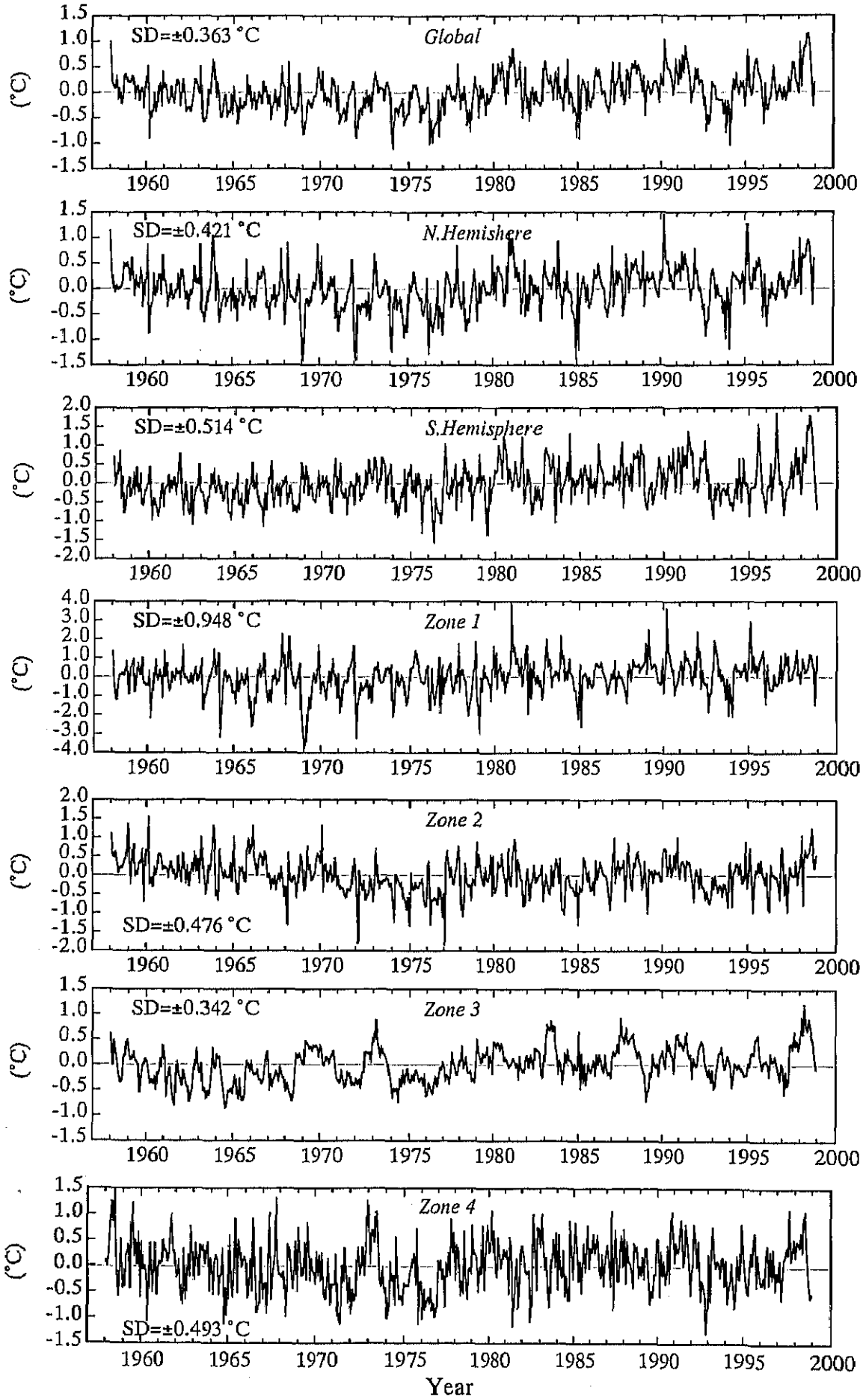

Fig.5-5. Anomalies in monthly mean land temperature for the period from 1958 to 1998 (data from NCEP/NCAR-reanalysis).

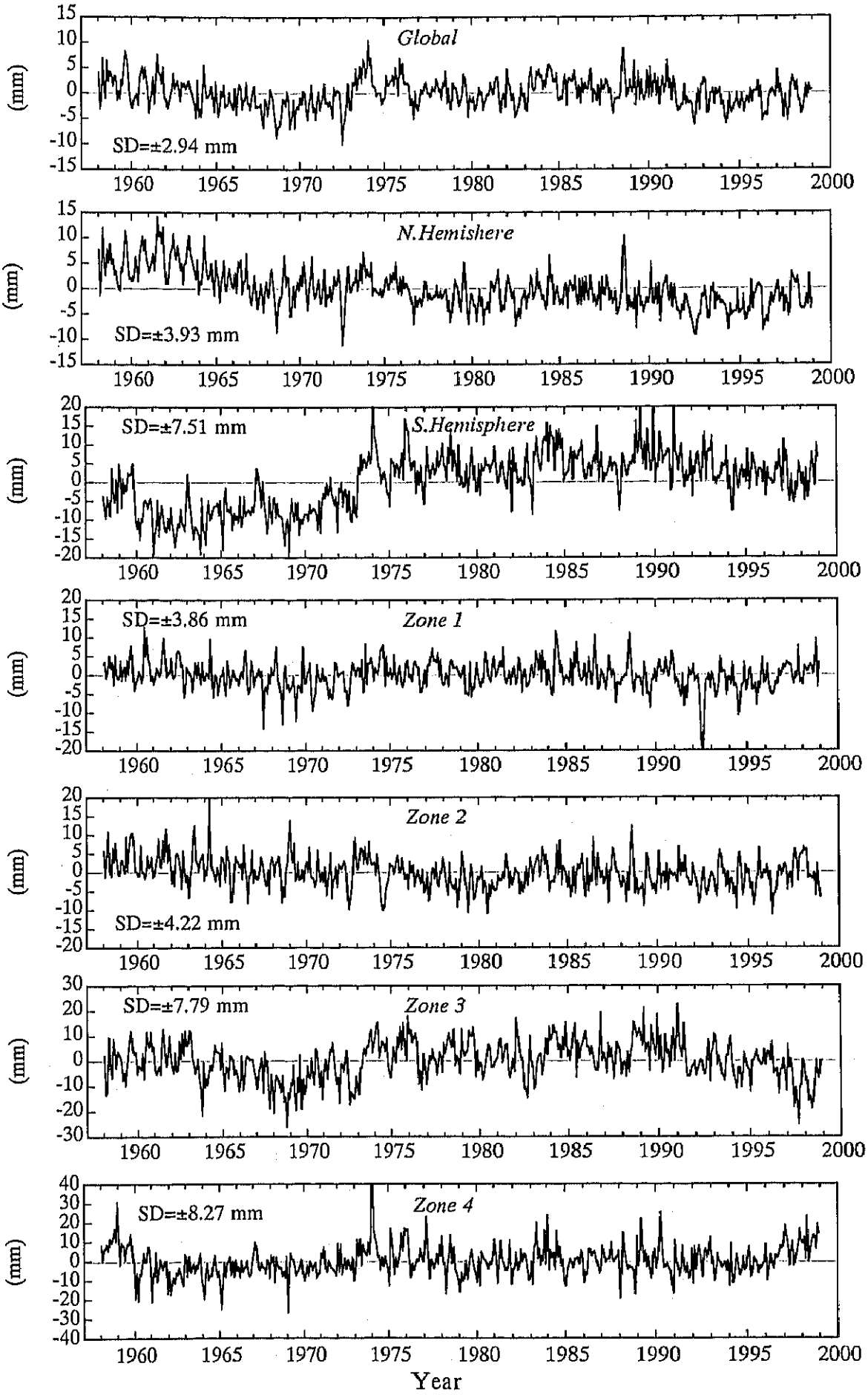

Fig.5-6. Anomalies in monthly mean land precipitation for the period from 1958 to 1998 (data from NCEP/NCAR-reanalysis).

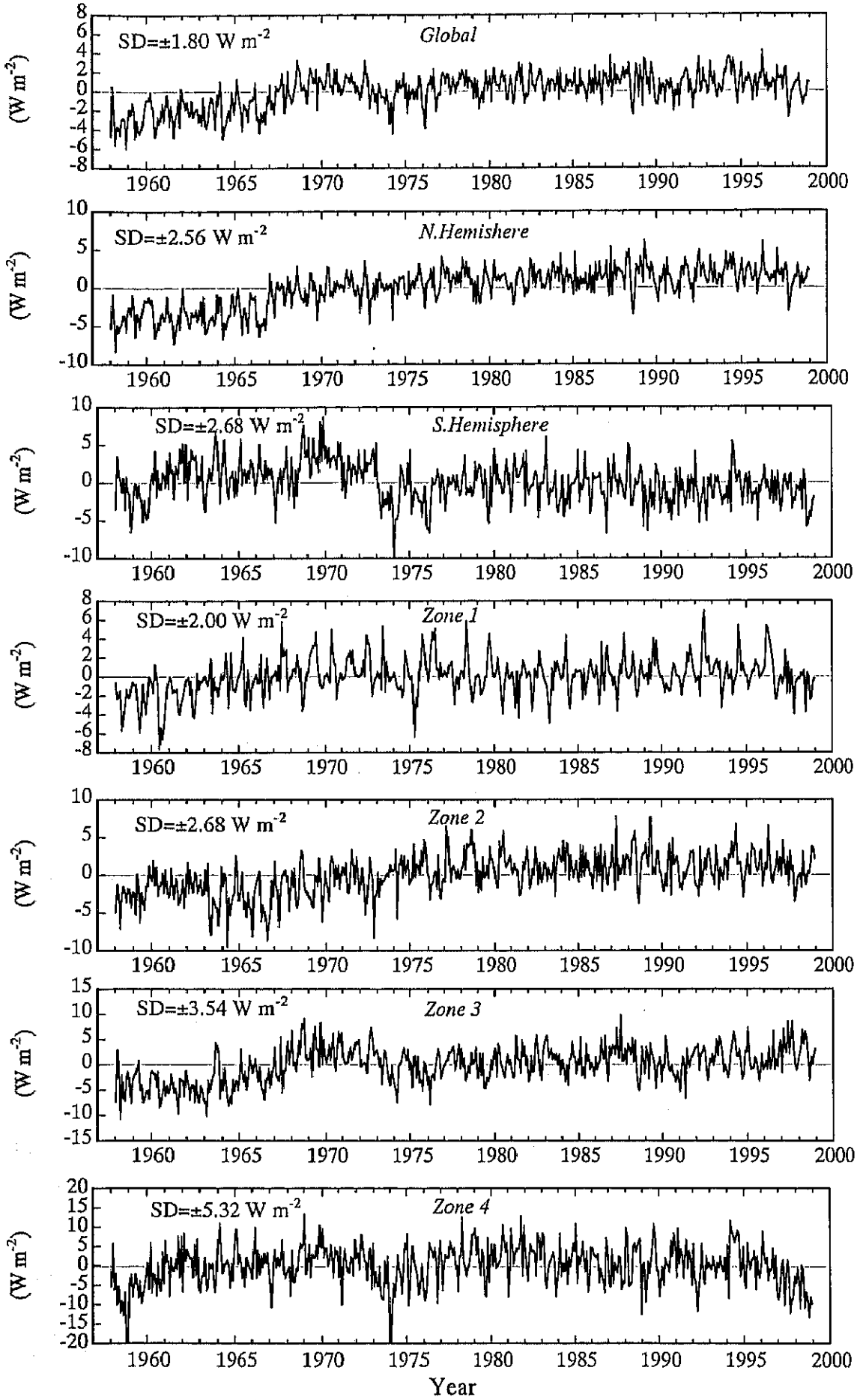

Fig.5-7. Anomalies in monthly mean land solar radiation for the period from 1958 to 1998 (data from NCEP/NCAR-reanalysis).

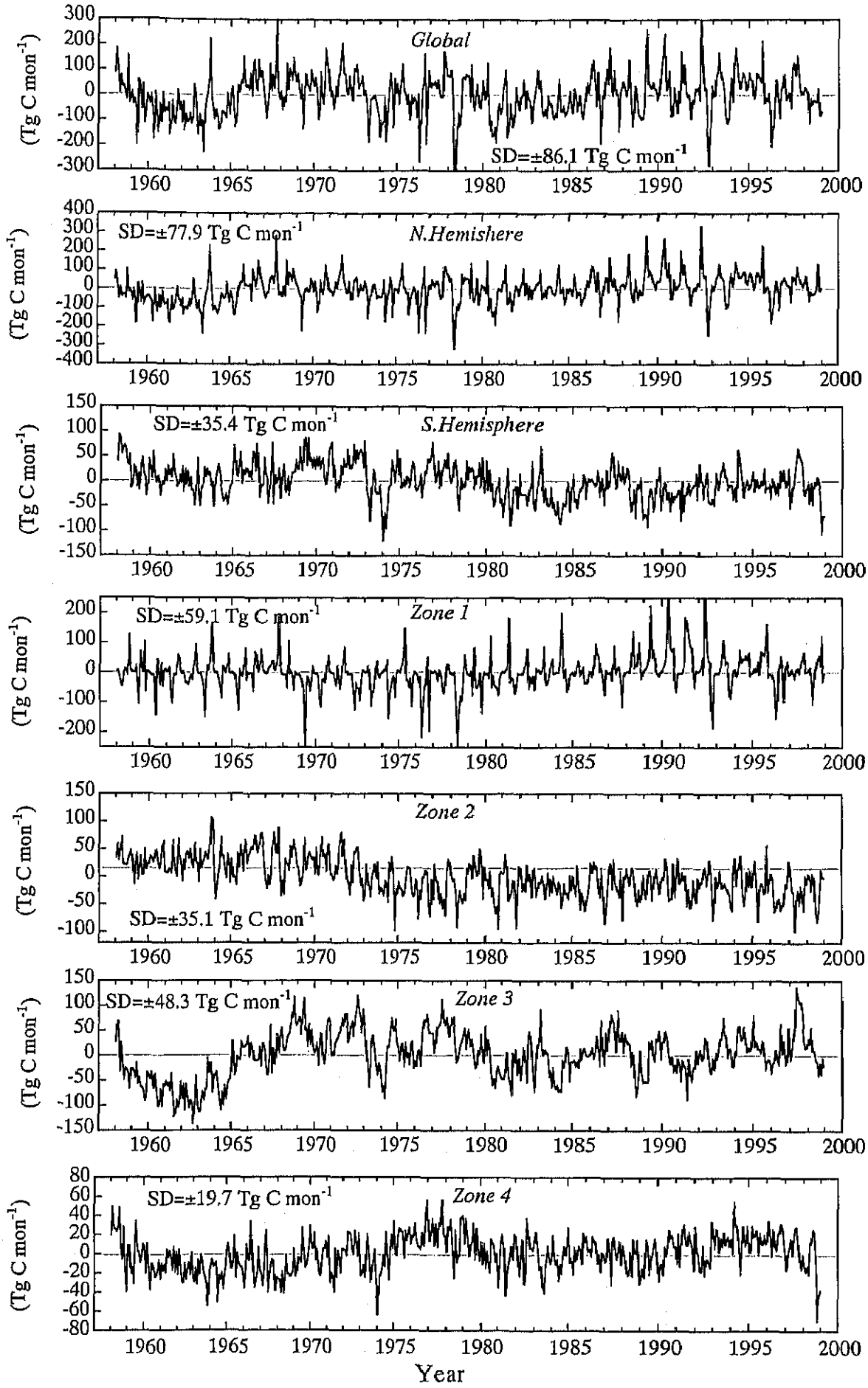

Fig.5-8. Anomalies in monthly gross photosynthetic production GPP for the period from 1958 to 1998.

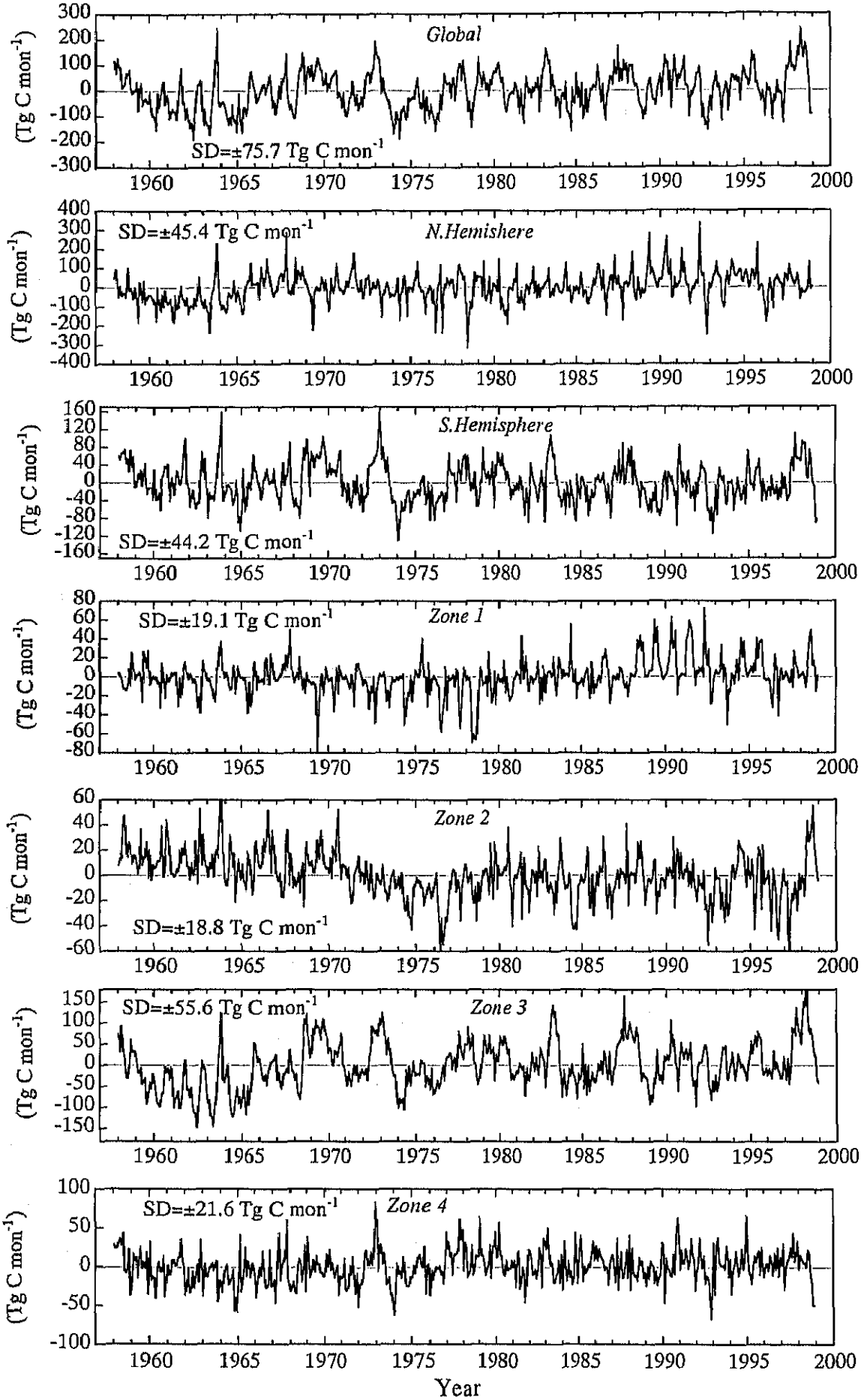

Fig.5-9. Anomalies in monthly plant autotrophic respiration AR for the period from 1958 to 1998.

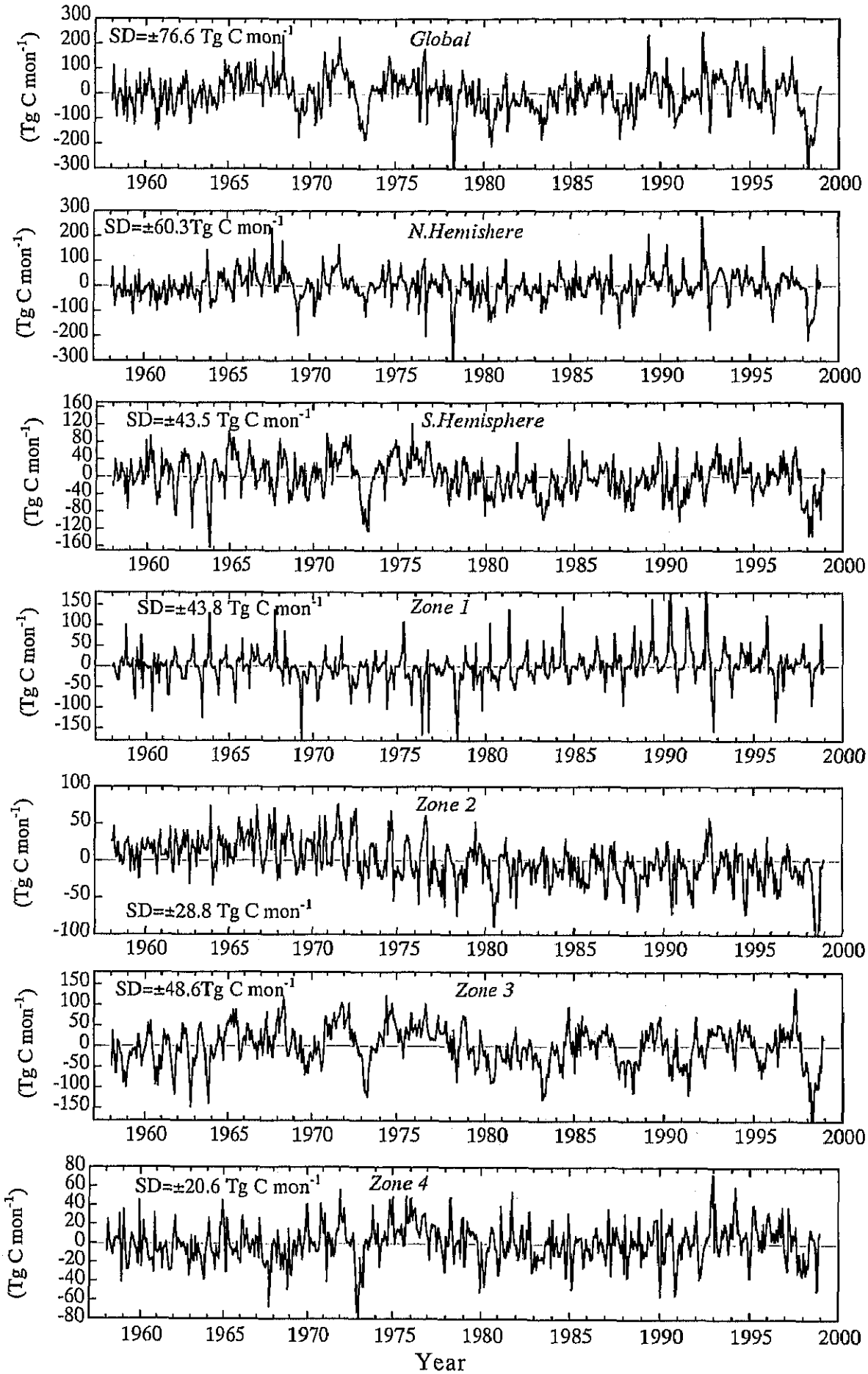

Fig.5-10. Anomalies in monthly net primary production *NPP* for the period from 1958 to 1998.

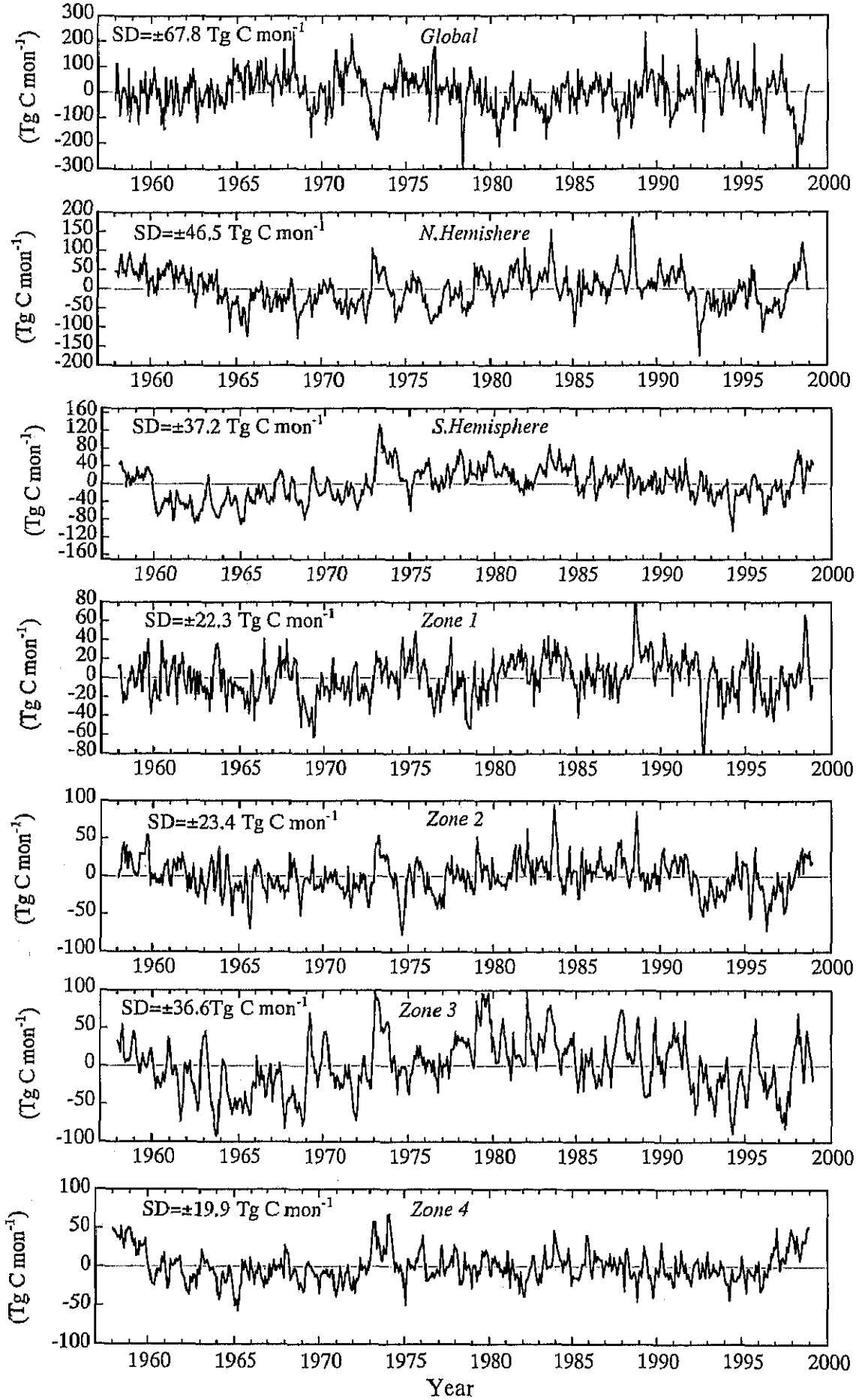

Fig.5-11. Anomalies in monthly soil heterotrophic respiration *HR* for the period from 1958 to 1998.

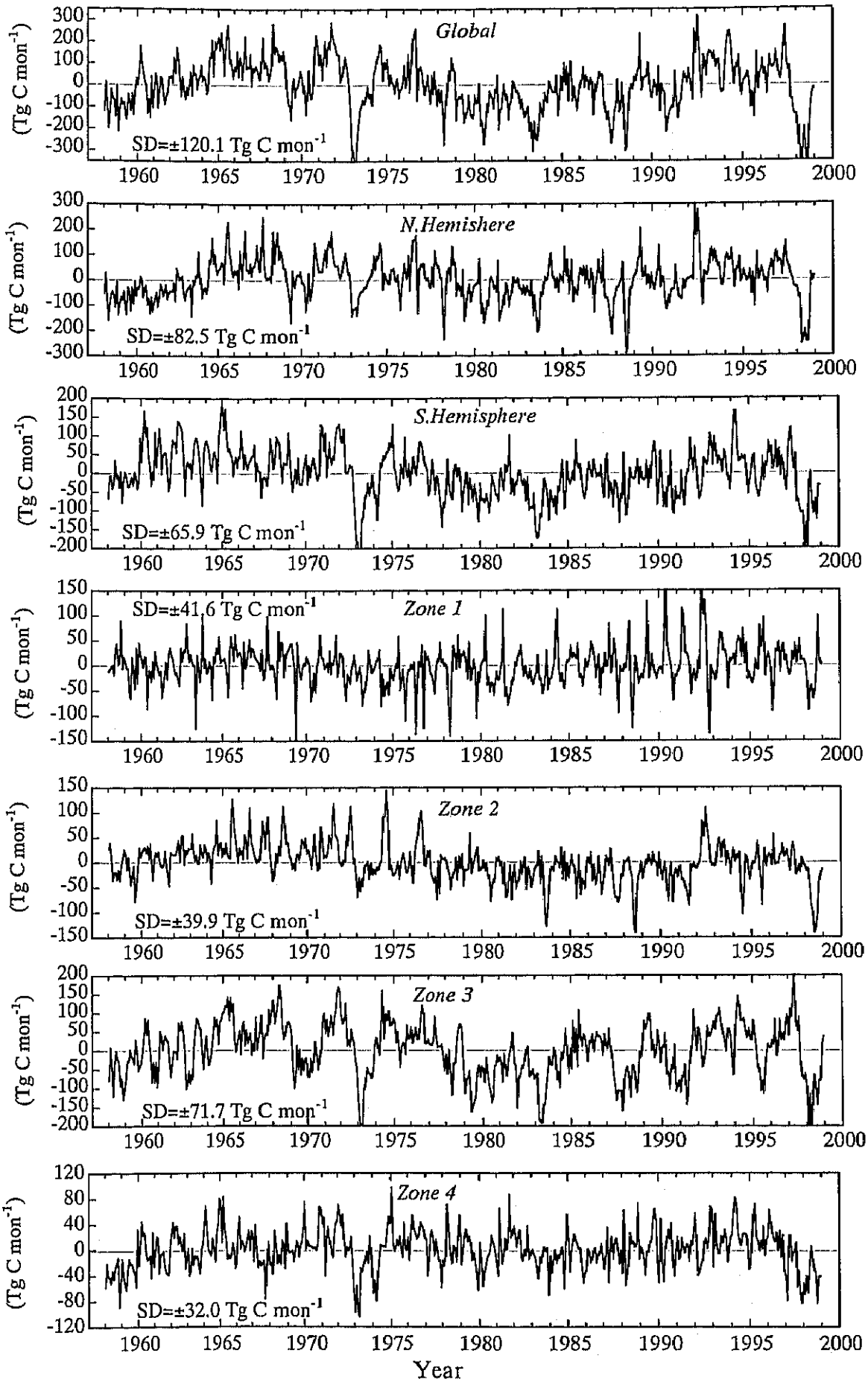

Fig.5-12. Anomalies in monthly net ecosystem production *NEP* for the period from 1958 to 1998.

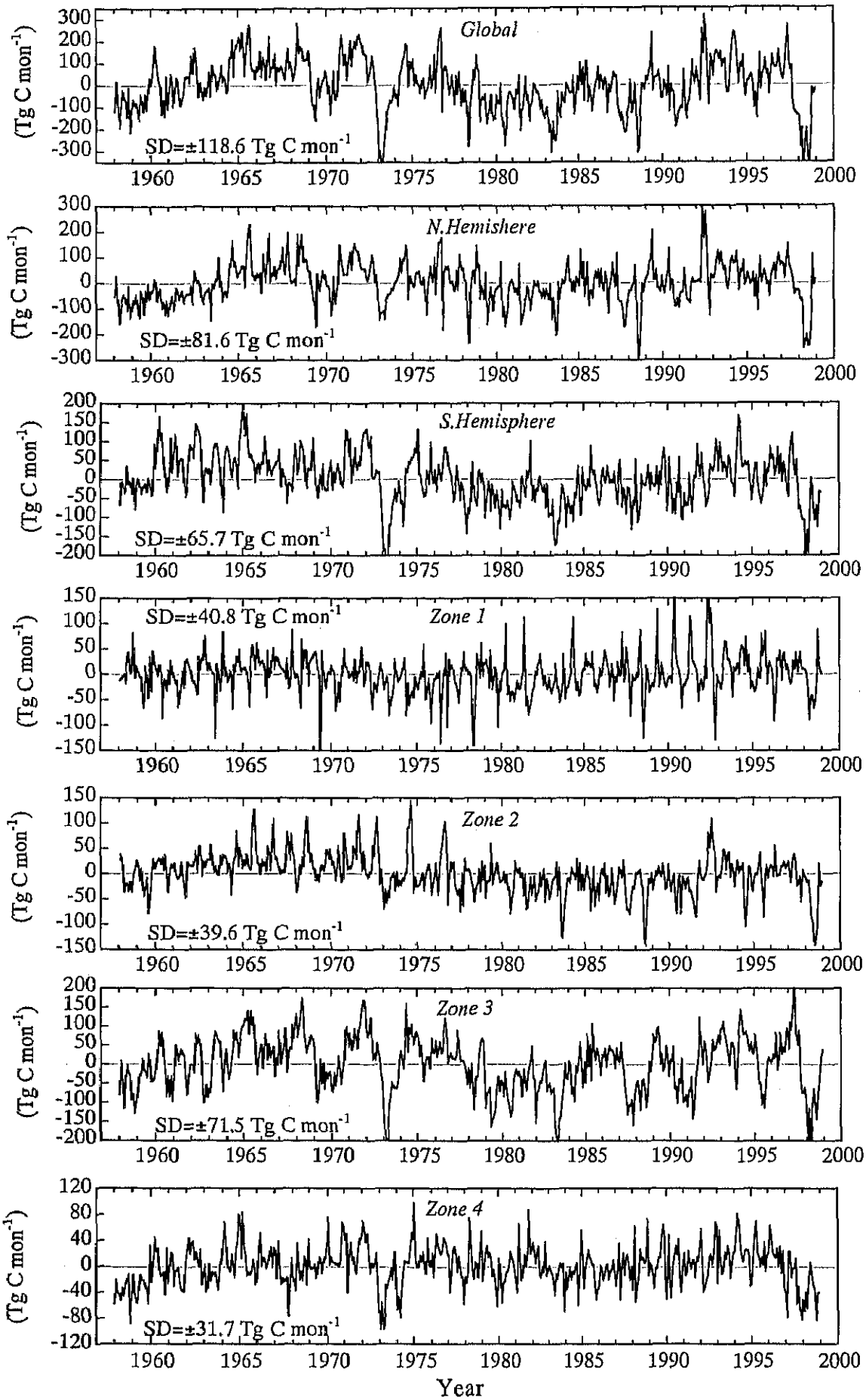

Fig.5-13. Anomalies in monthly net ecosystem carbon balance *NCB* for the period from 1958 to 1998.

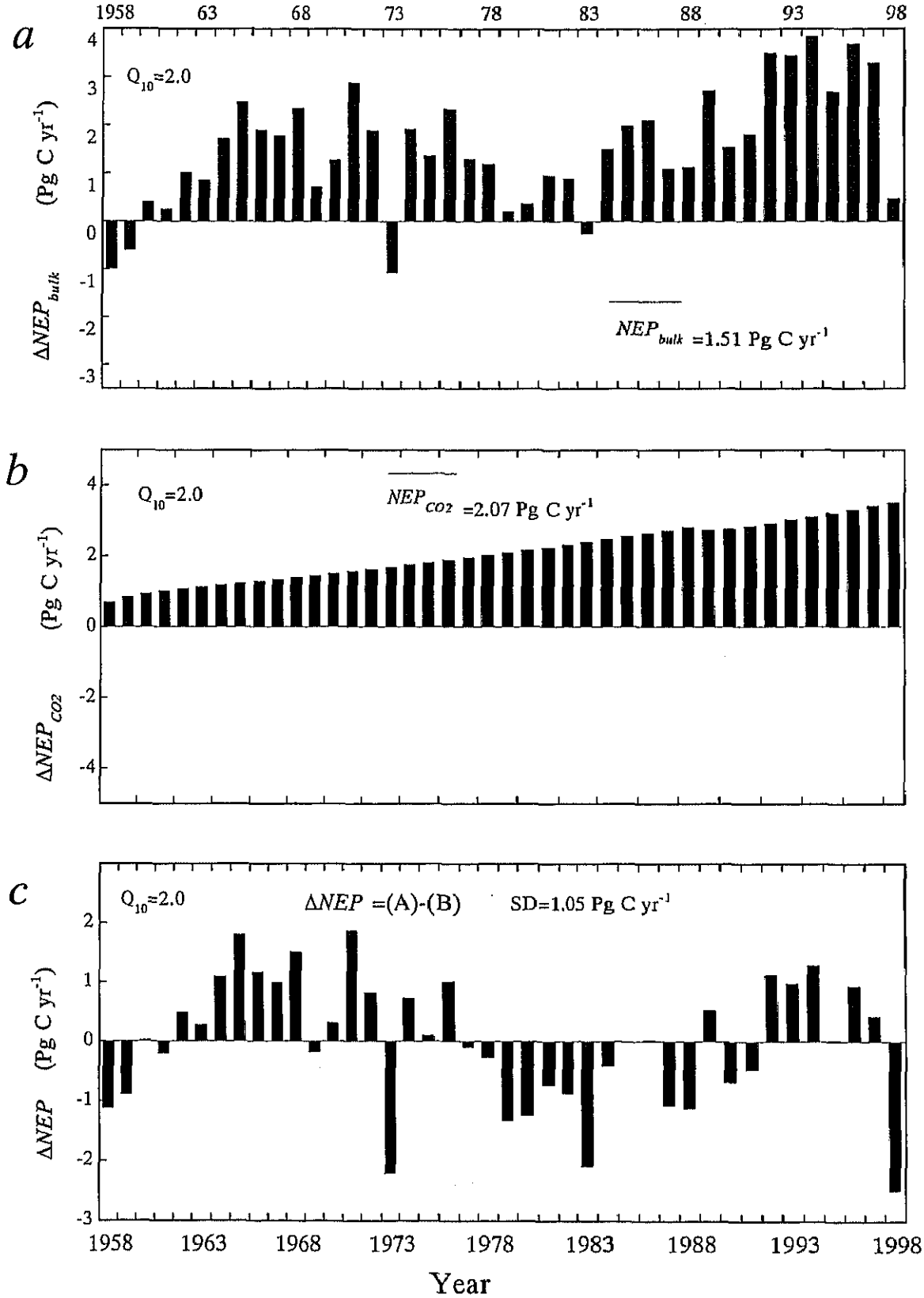

Fig. 5-14. Annual *NEP* anomalies estimated by Sim-CYCLE 41-year run.

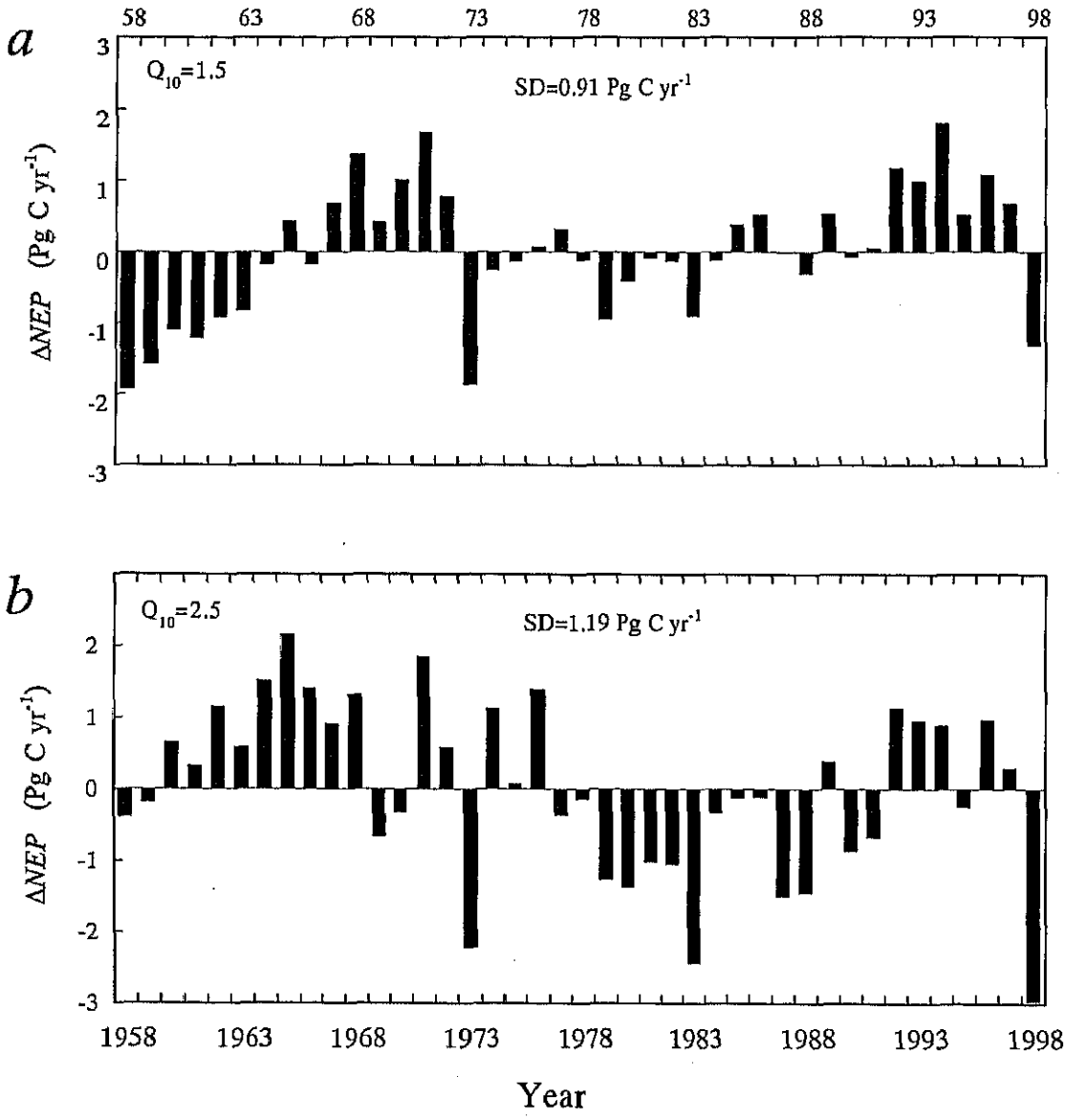

Fig. 5-15. Annual ΔNEP using different values for temperature dependence of respirations, (a) 1.5 and (b) 2.5.

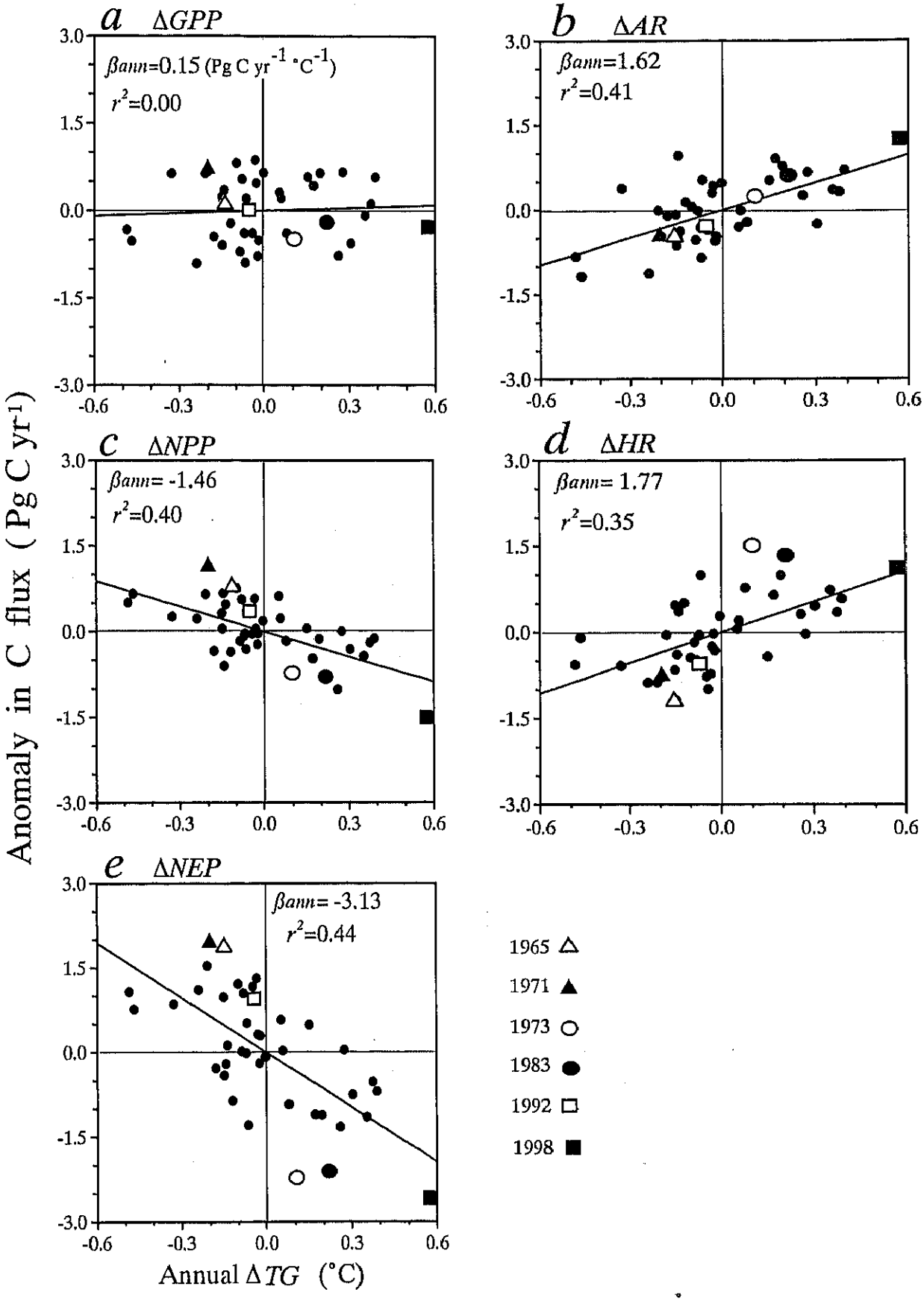

Fig. 5-16. Correlations between ΔTG and carbon flux anomalies.

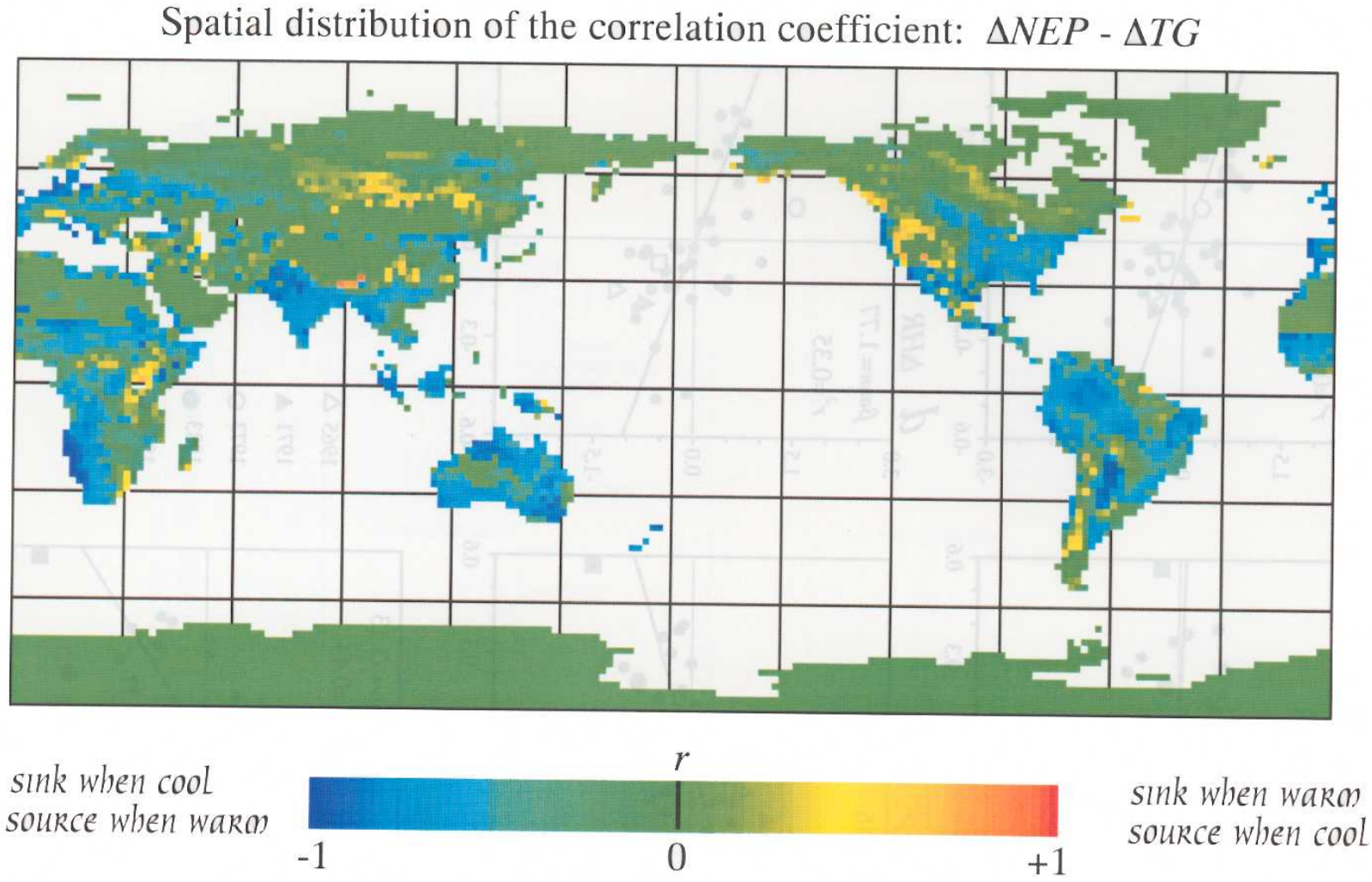

Fig. 5-17. Distribution of correlation coefficient between the anomaly of surface temperature ΔTG and the anomaly of estimated carbon budget ΔNEP, at annual base.

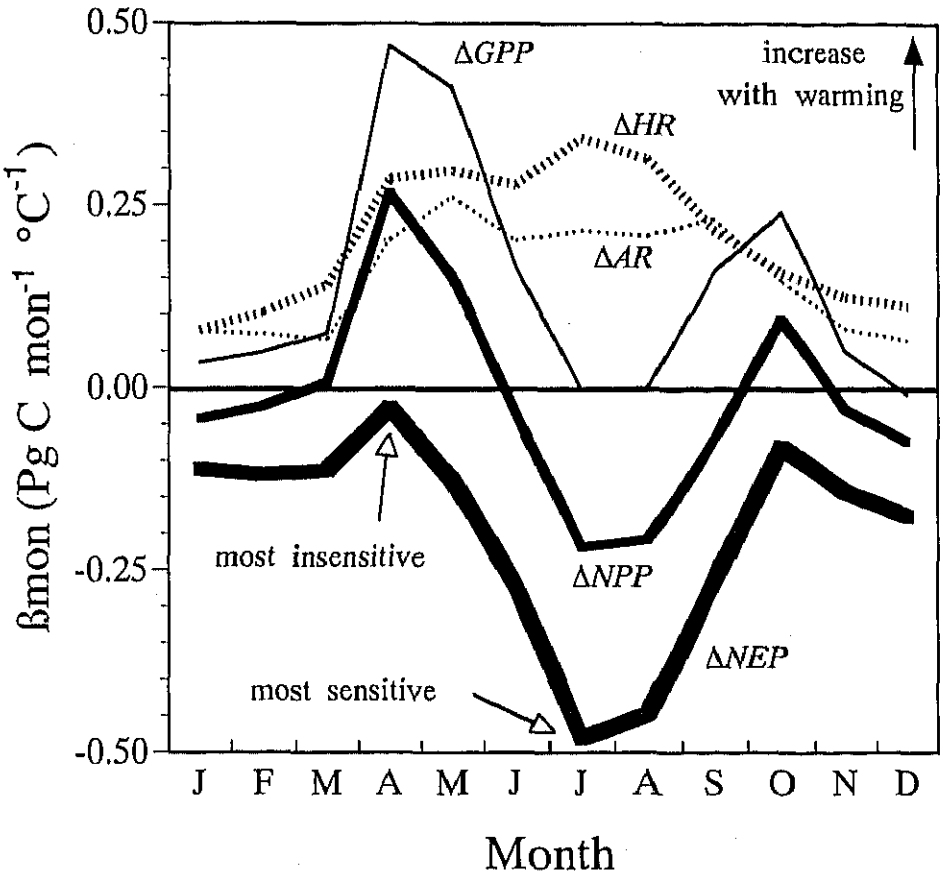

Fig. 5-18. Seasonal change in the slope of regresstion between ΔTG and carbon flux anomalies.

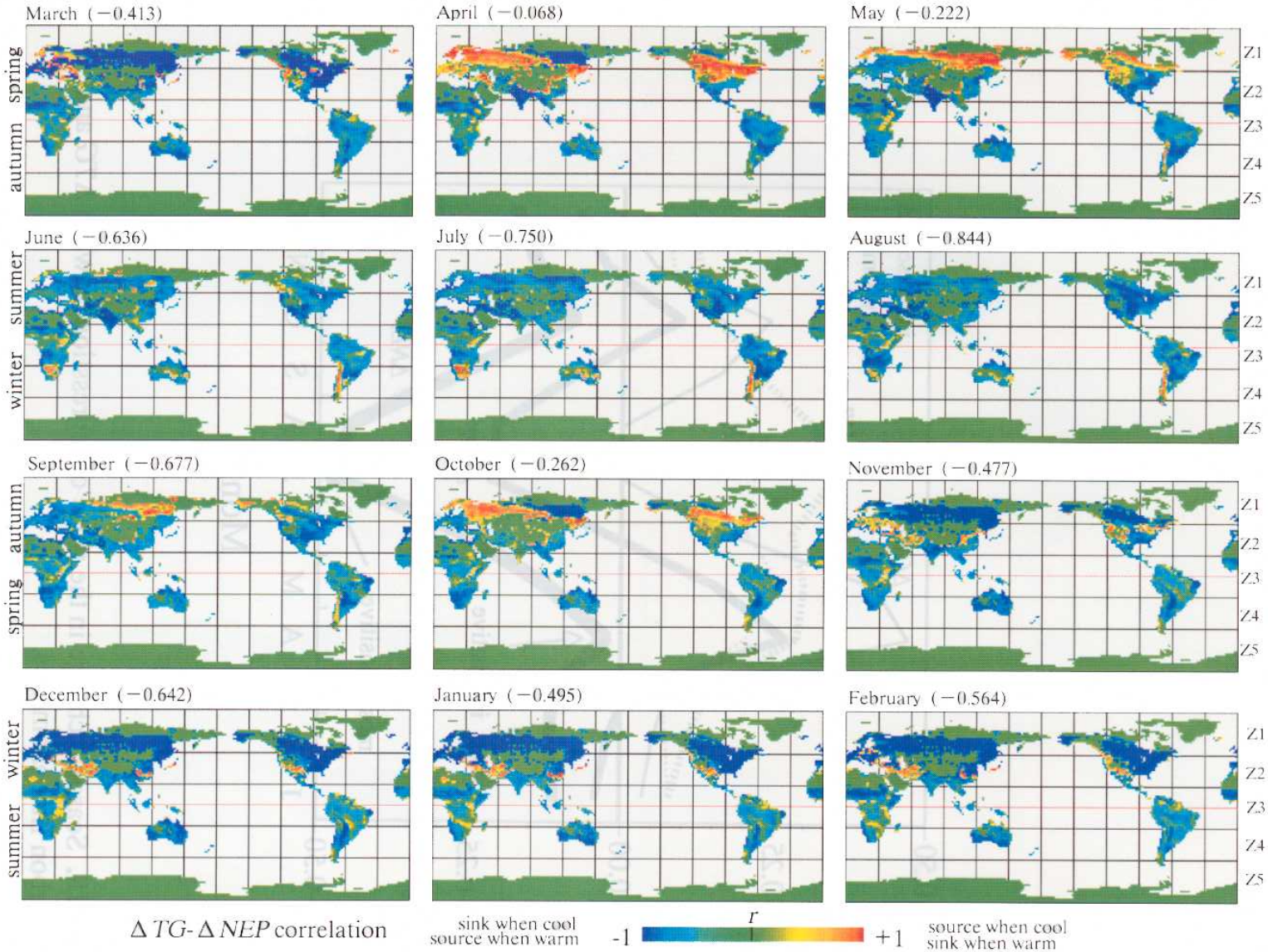

Fig. 5-19. Seasonal change in the distribution of correlation coefficient (r) between ΔTG and ΔNEP.

(mass in Pg C, flux in Pg C yr^{-1}, (anomaly))

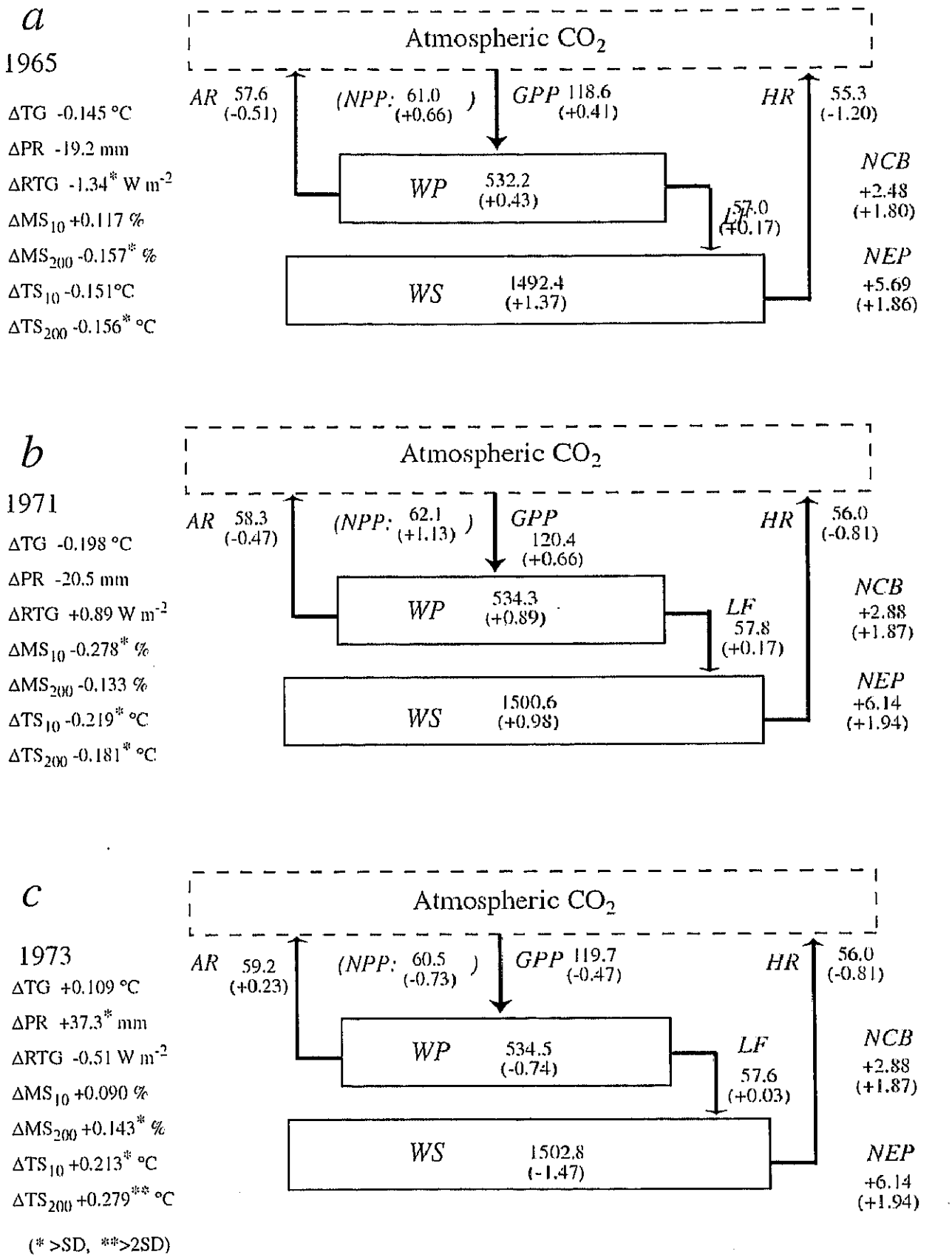

Fig. 5-20. Biospheric carbon dynamics estimated by Sim-CYCLE 41-year run, in case of (a) 1965, (b) 1971, and (c) 1973.

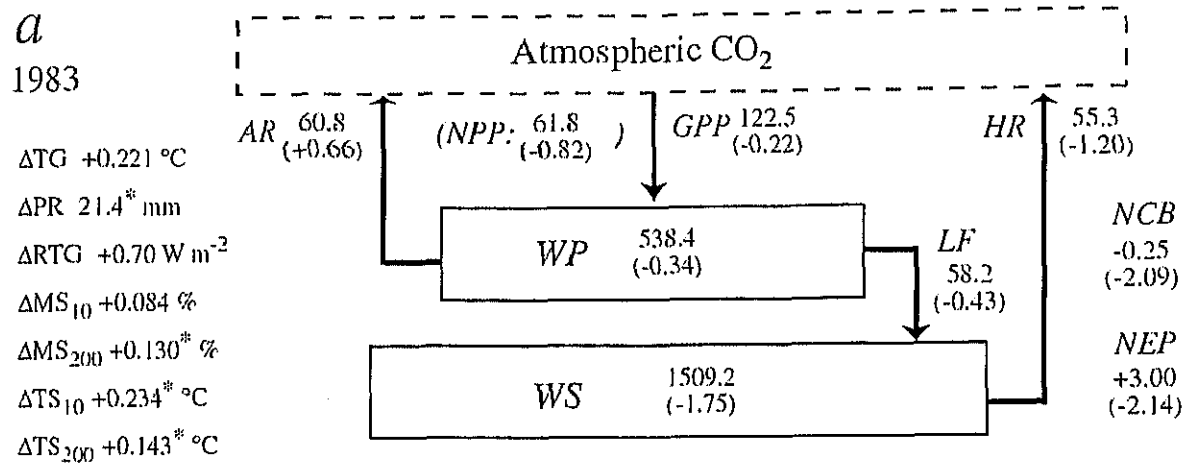

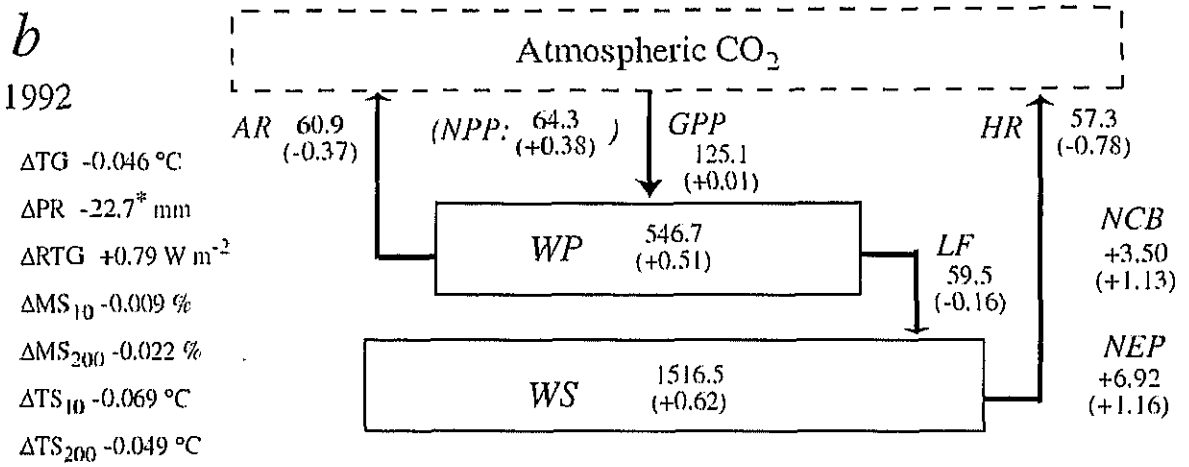

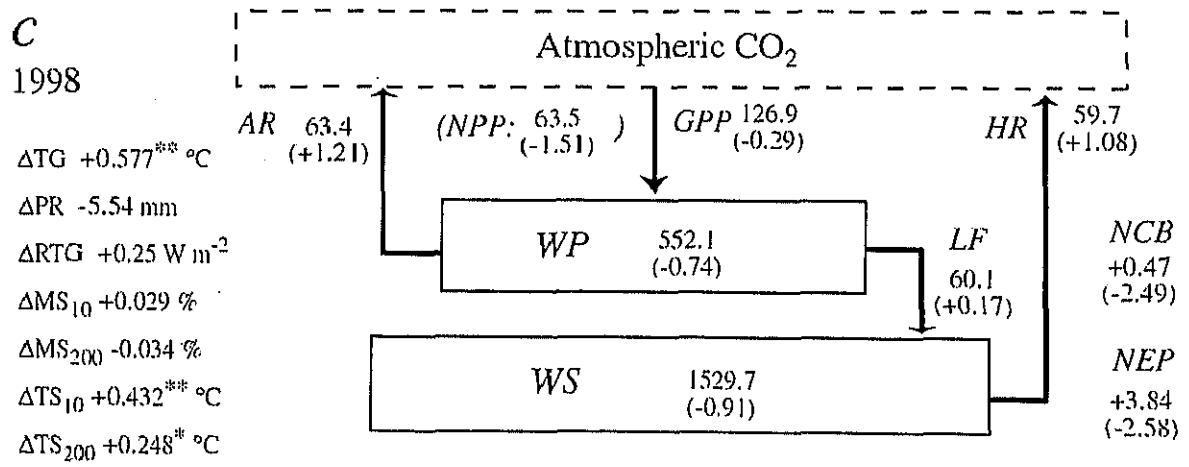

Fig. 5-20 (continued). Biospheric carbon dynamics estimated by Sim-CYCLE 41-year run, in case of (a) 1983, (b) 1992, and (c) 1998.

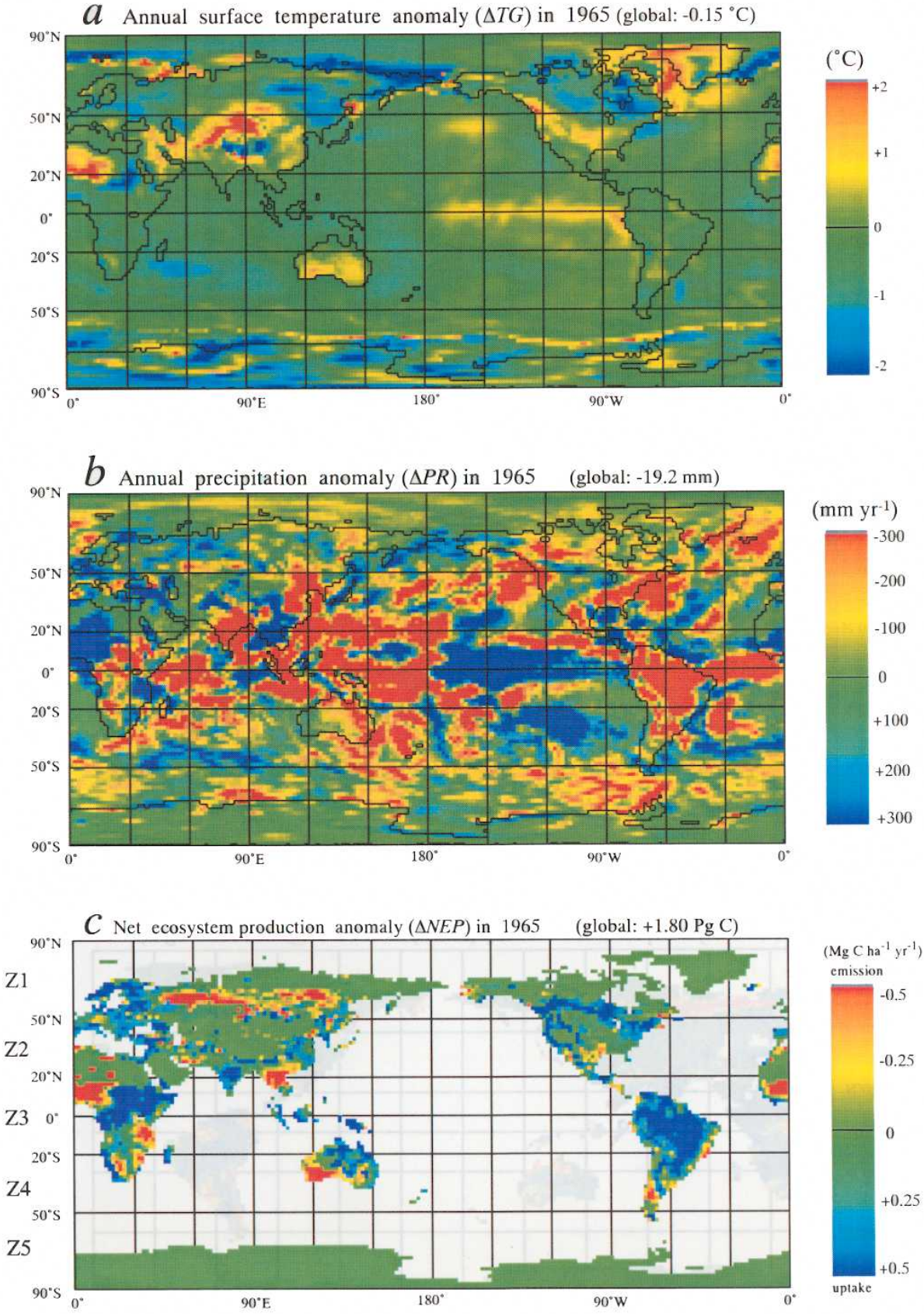

Fig. 5-21. Anomalies in (a) annual mean surface temperature, (b) annual precipitation, and (c) and annual *NEP*estimated by the Sim-CYCLE 41-year simulation analysis. The features in 1965 are shown.

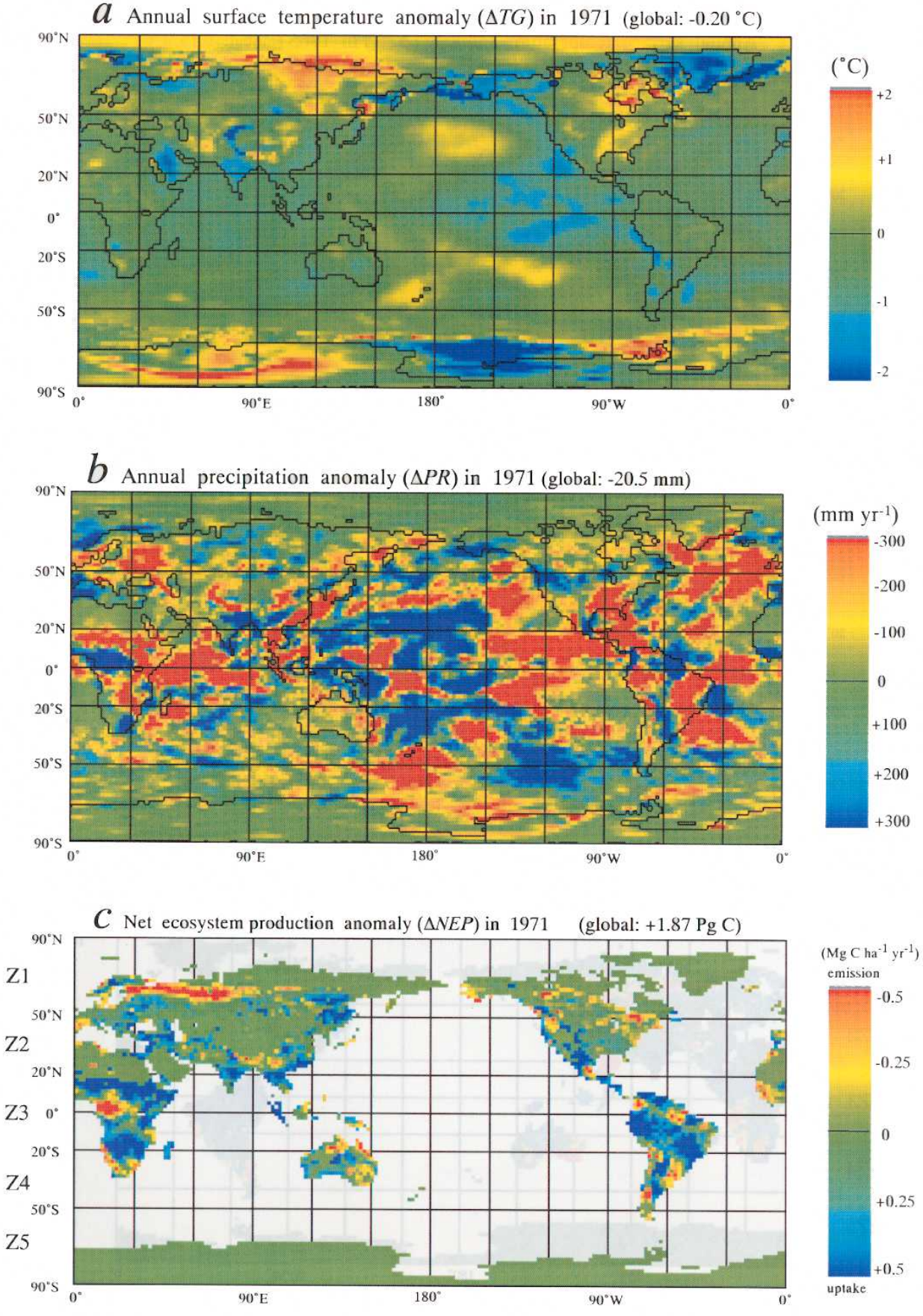

Fig. 5-22. Similar to Fig. 5-21, but anomalies in 1971 are shown.

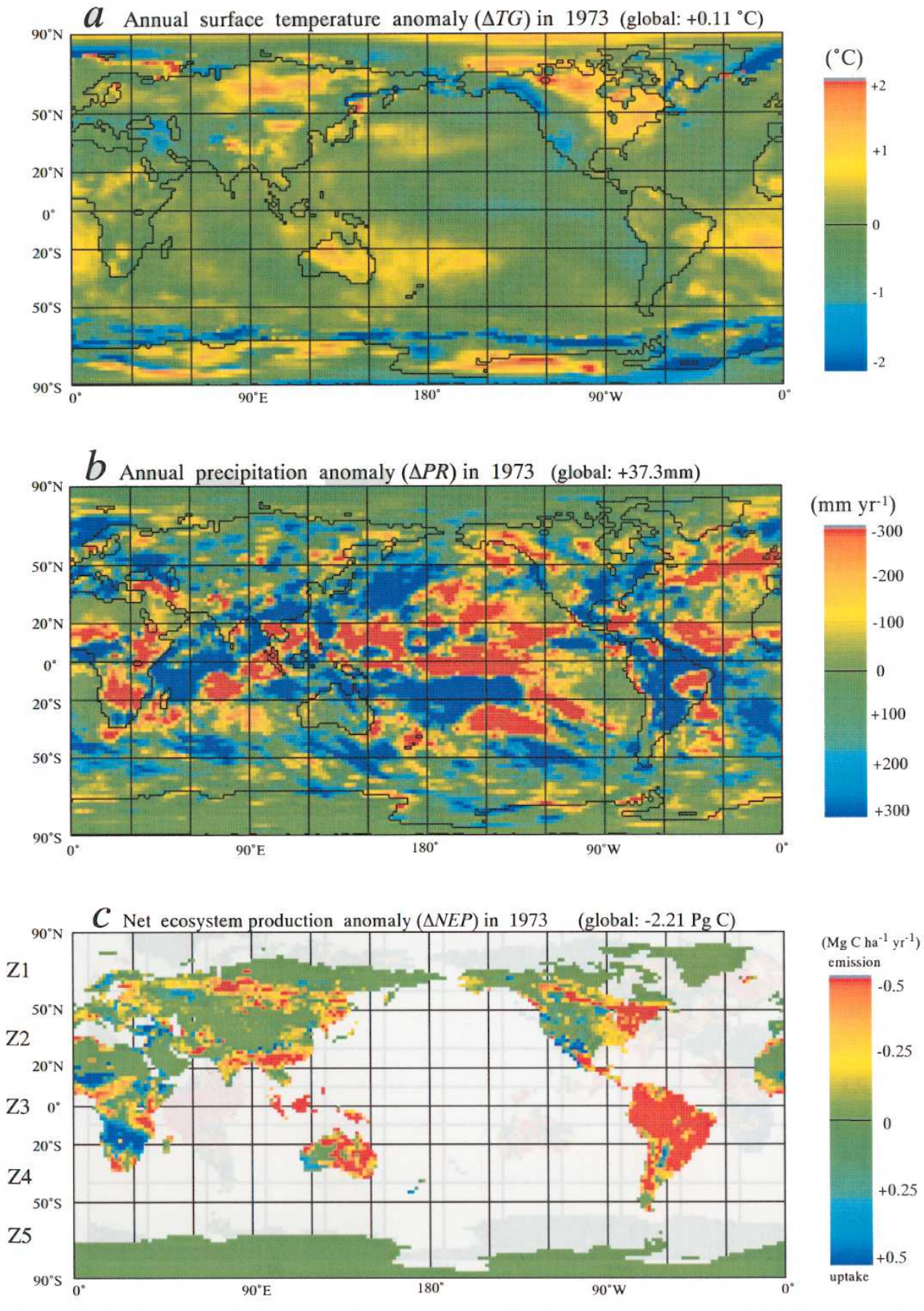

Fig. 5-23. Similar to Fig. 5-21, but anomalies in 1973 are shown.

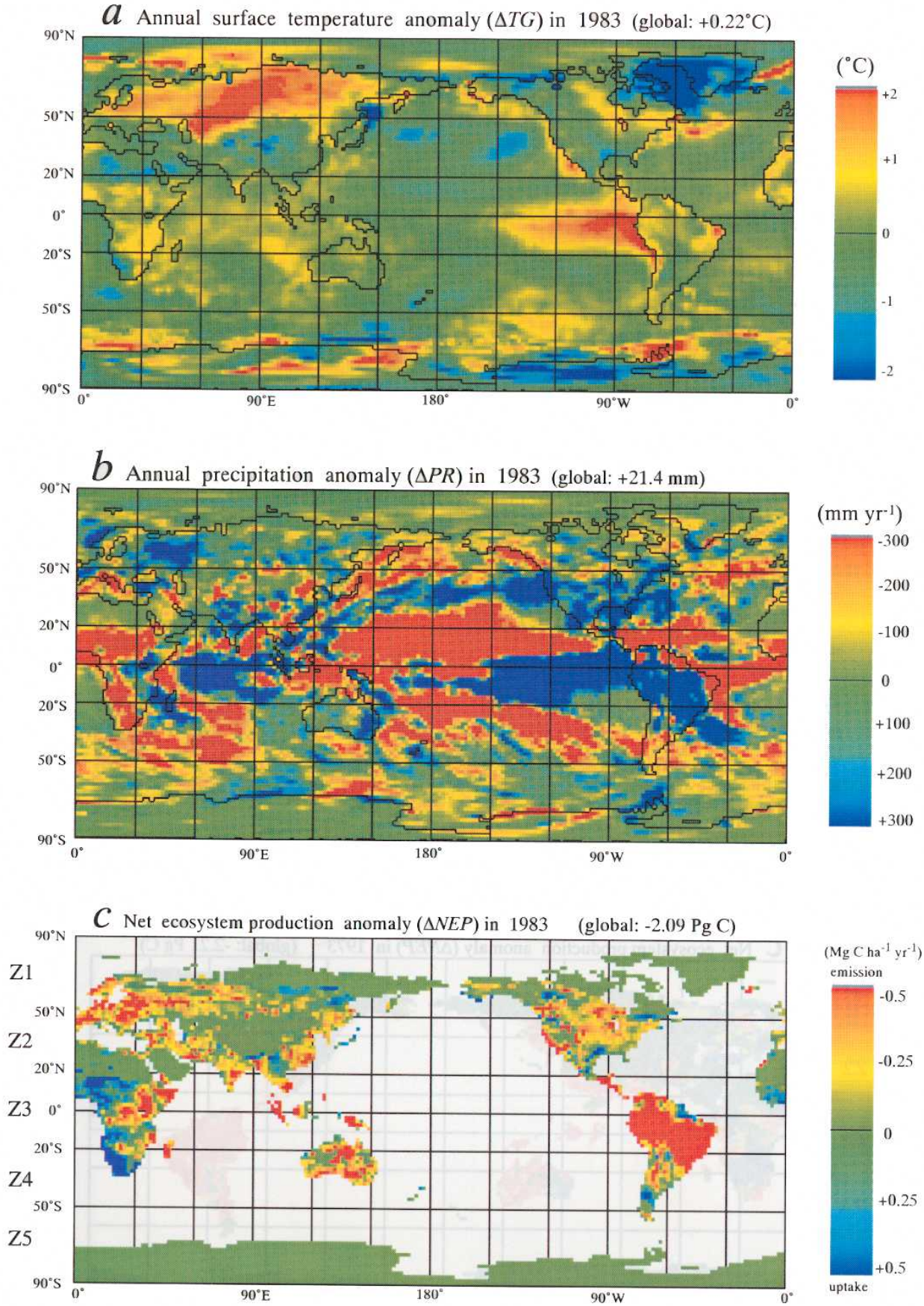

Fig. 5-24. Similar to Fig. 5-21, but anomalies in 1983 are shown.

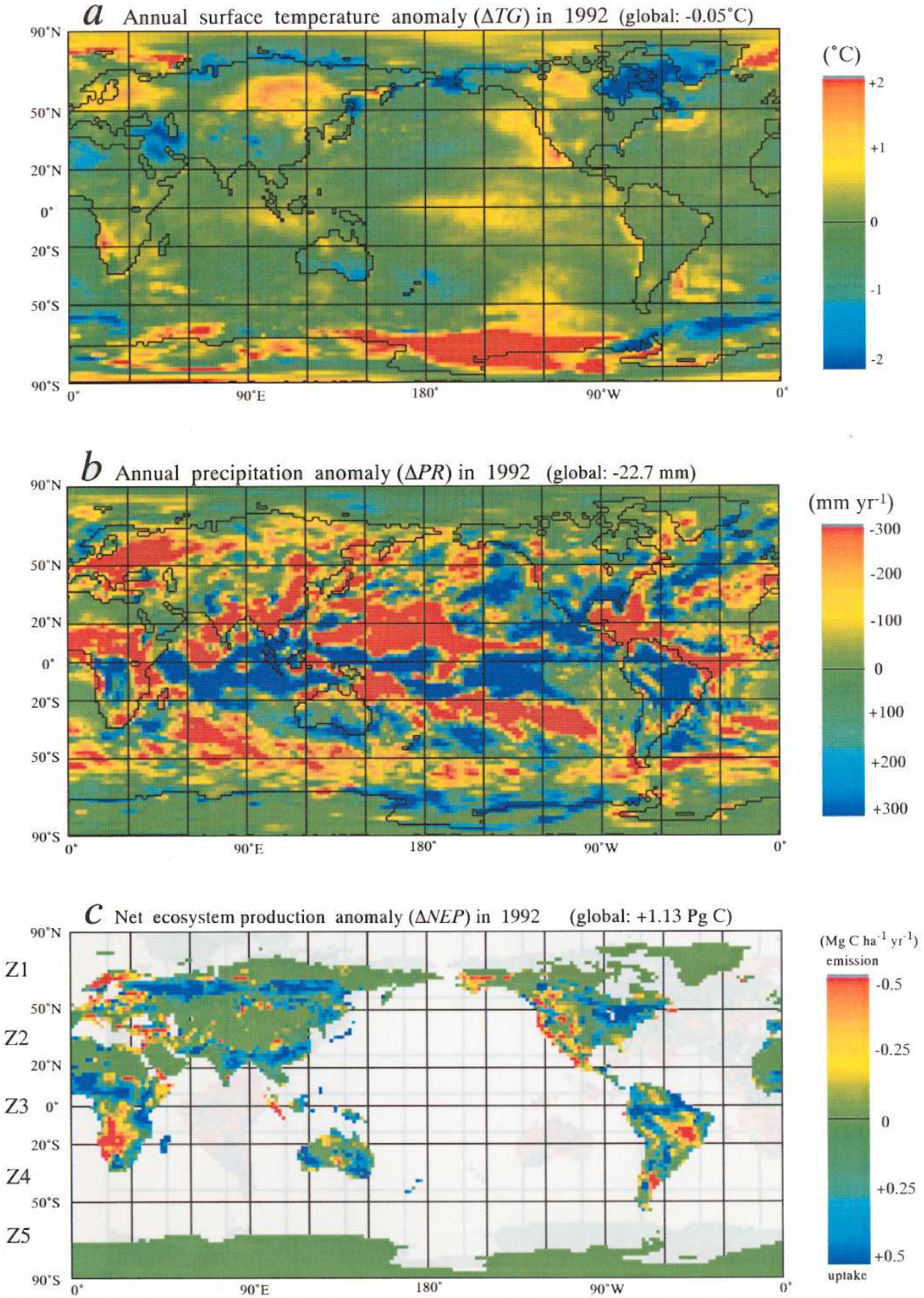

Fig. 5-25. Similar to Fig. 5-21, but anomalies in 1992 are shown.

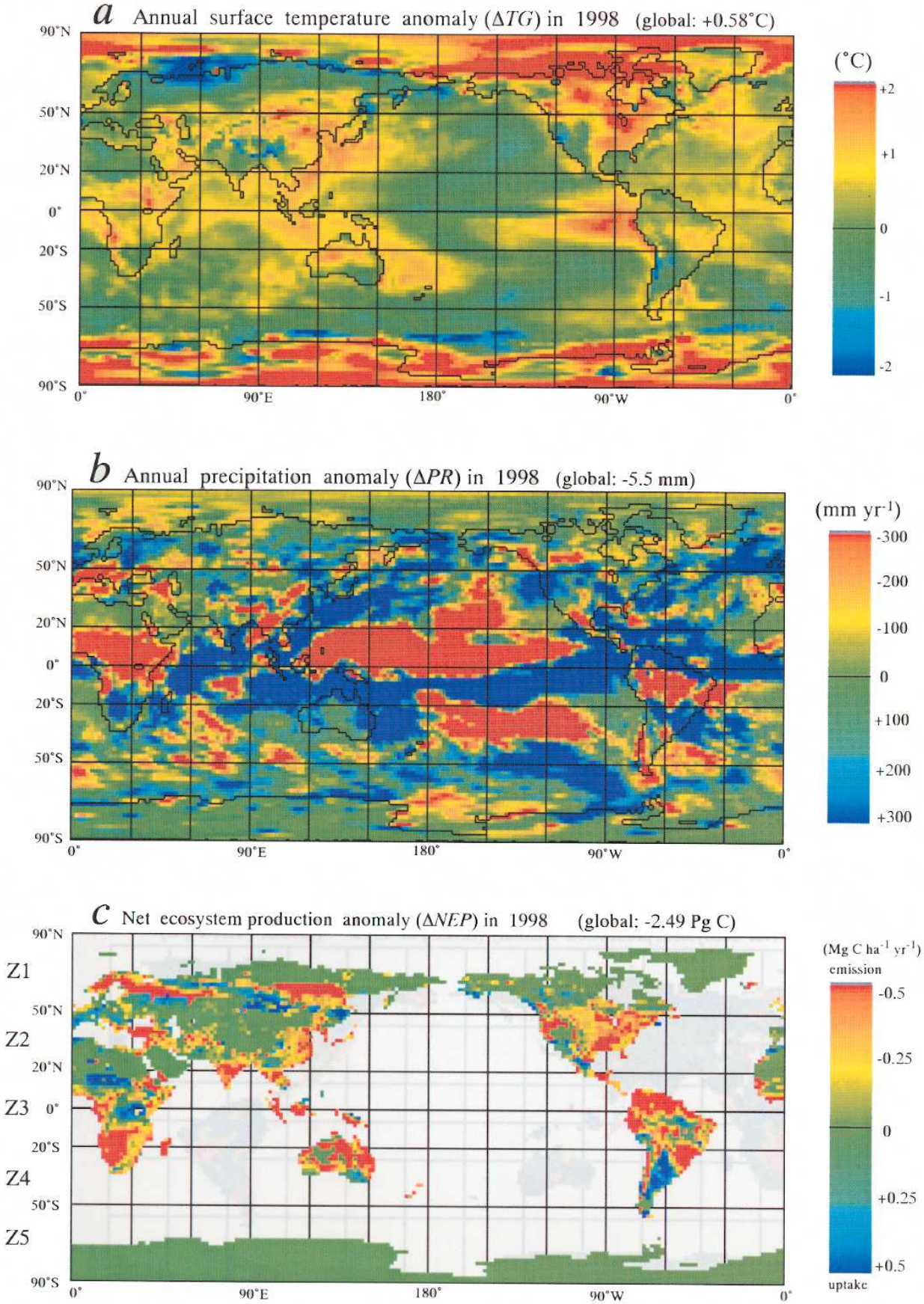

Fig. 5-26. Similar to Fig. 5-21, but anomalies in 1998 are shown.

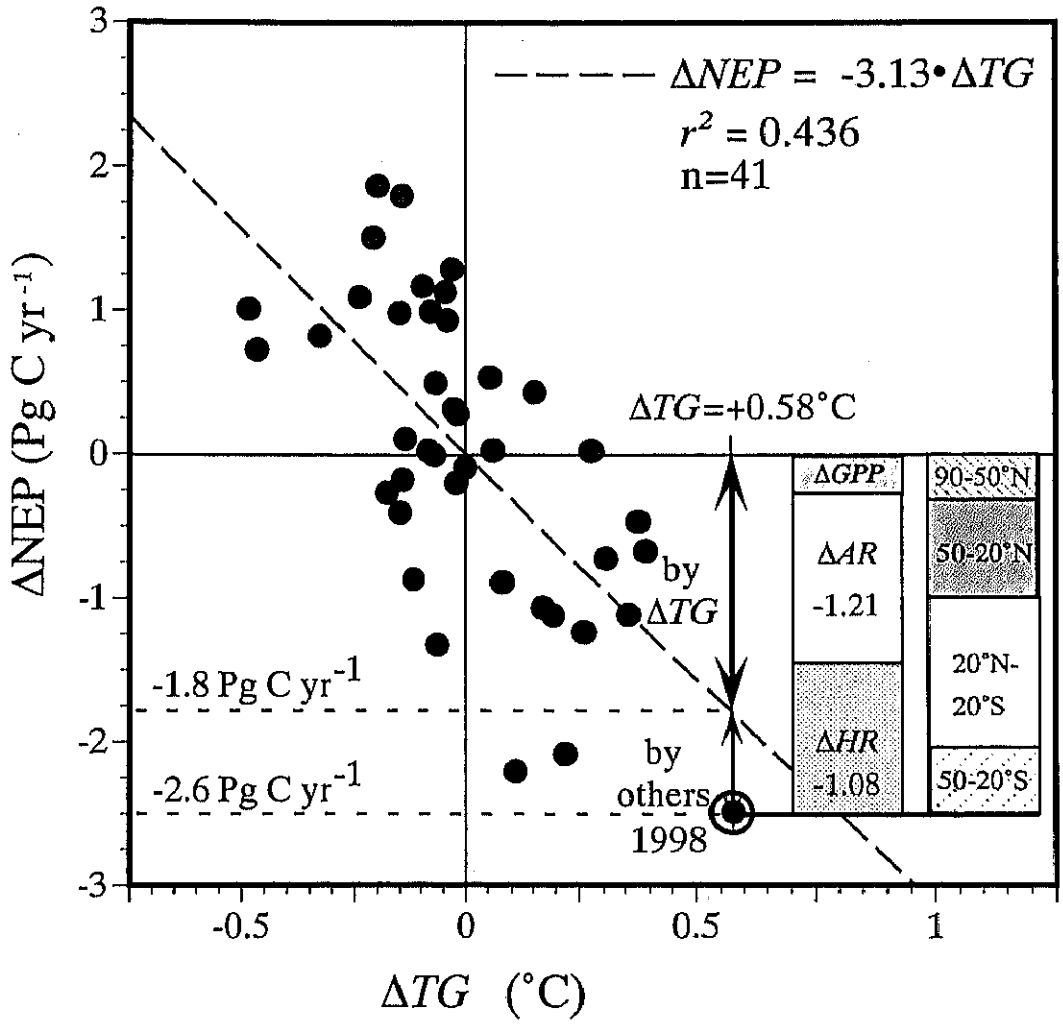

Fig. 5-27. Relationship between ΔTG and ΔNEP, exemplified for the year 1998

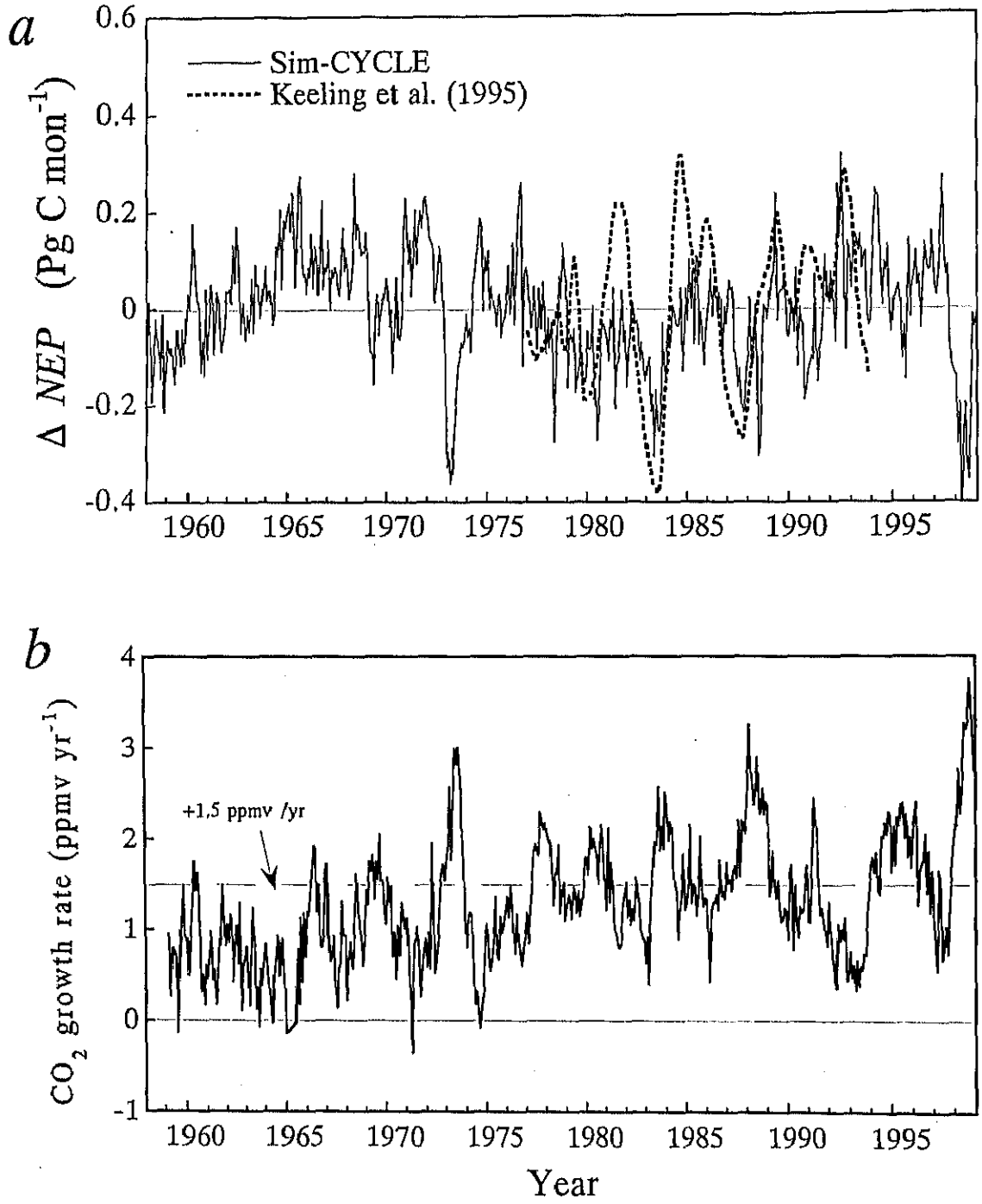

Fig. 5-28. Time-series of (a) net biospheric CO_2 budget and (b) increase rate of atmospheric CO_2 concentration.